

This is a preprint version of the article published in:

Composites Part B: Engineering, Vol. 220 (2021), 109006.

<https://doi.org/10.1016/j.compositesb.2021.109006>

Please, cite this document as:

R. Venegas, T. G. Zieliński, G. Núñez, F.-X. Bécot, “Acoustics of porous composites.” *Composites Part B: Engineering*, Vol. 220 (2021), 109006. DOI: [10.1016/j.compositesb.2021.109006](https://doi.org/10.1016/j.compositesb.2021.109006)

Acoustics of porous composites

RODOLFO VENEGAS^{1a} TOMASZ G. ZIELIŃSKI^{2b} GABRIEL NÚÑEZ^{3a} FRANÇOIS-XAVIER BÉCOT^{4c}

^a*University Austral of Chile, Institute of Acoustics, P.O. Box 567, Valdivia, Chile*

^b*Institute of Fundamental Technological Research, Polish Academy of Sciences, ul. Pawińskiego 5B, 02-106 Warsaw, Poland*

^c*MATELYS – Research Lab, 7 rue des Maraîchers (bâtiment B), F69120 Vaulx-en-Velin, France*

Abstract

Acoustic wave propagation in porous composites is investigated in this paper. The two-scale asymptotic homogenisation method is used to obtain the macroscopic description of sound propagation in such composites. The developed theory is both exemplified by introducing analytical models for the effective acoustical properties of porous composites with canonical inclusion patterns (i.e. a porous matrix with a periodic array of cylindrical or spherical inclusions) and validated by comparing the models predictions with the results of direct finite-element simulations and experimental testing, showing good agreement in all cases. It is concluded that the developed theory correctly captures the acoustic interaction between the constituents of the porous composite and elucidates the physical mechanisms underlying the dissipation of sound energy in such composites. These correspond to classical visco-thermal dissipation in the porous constituents, together with, for the case of composites made from constituents characterised by highly contrasted permeabilities, pressure diffusion which provides additional and tunable sound energy dissipation. In addition, this work determines the conditions for which a rigidly-backed porous composite layer can present improved sound absorption performance in comparison with that of layers made from their individual constituents. Hence, the presented results are expected to guide the rational design of porous composites with superior acoustic performance.

Key words: Porous composites; Wave propagation; Acoustical properties; Homogenisation; Pressure diffusion.

¹rodolfo.venegas@uach.cl (Corresponding Author)

²tzielins@ippt.pan.pl

³gabriel.nunez@alumnos.uach.cl

⁴fxb@matelys.com

1 Introduction

Gas-saturated conventional permeable materials, such as porous, fibrous, granular and cellular materials [1, 2], play a key role in improving indoor sound quality [3] (e.g. in classrooms, concert venues, buildings) and reducing noise [1, 3] in vehicles and outdoors thanks to their capability to attenuate sound due to gas viscosity and heat exchanges between their solid frame and saturating fluid [1, 4–11]. In these materials, one can identify microstructural parameters, namely, a local characteristic length, ℓ , and a single porosity (i.e. the fraction of the voids volume over the total material volume) that determine their acoustic properties; as well as a macroscopic characteristic length L determined by the sample size or a characteristic length of a physical phenomenon, e.g. the sound wavelength λ .

In the long-wavelength regime, i.e. $\lambda \gg \ell$, and provided that the solid frame can be assumed motionless because either the frame is much heavier or stiffer than the saturating fluid, conventional single porosity materials (SPM) can be modelled as equivalent visco-thermal fluids with effective parameters [1, 6–8, 10, 11]. This well established modelling approach can be rigorously justified via upscaling techniques [6, 10] such as the two-scale asymptotic method of homogenisation [11, 12], which is a technique to be used in this paper and will be referred to, for short, as homogenisation.

Homogenisation is a mathematical technique concerned with the derivation of macroscopic models, valid at a scale much larger than that of the local heterogeneities, of physical phenomena occurring at the local scale. It relies on the concept of separation of scales (i.e. $\ell/L \ll 1$ in acoustics) and its goal is to describe a heterogeneous medium as an equivalent continuum with effective parameters that encapsulate the influence of the local physics on the medium's macroscopic properties. Thus, homogenisation links the large-scale observable behaviour to microscopic mechanisms governed by a set of equations formulated at the local scale and known as local description.

For acoustic wave propagation in SPM with a rigid frame, the local description is formulated in the pore fluid network of a representative elementary volume (REV) of the material and corresponds to the Stokes-Fourier system, which comprises the linearised equations of conservation of momentum, mass, energy, and the equation of state; together with the no-slip and zero temperature excess conditions set on the heterogeneities boundaries. Applying homogenisation (see e.g. [11]) leads to the frequency-domain effective model given by the mass balance equation (1) and fluid flow constitutive law or dynamic Darcy's law (2), i.e.

$$\nabla \cdot \mathbf{V} + j\omega p C(\omega) = 0, \quad (1)$$

$$\mathbf{V} = -\frac{\mathbf{k}(\omega)}{\eta} \cdot \nabla p, \quad (2)$$

where ∇ is the vector differential operator, \mathbf{V} is the mean fluid velocity, p is the acoustic pressure, η is the dynamic viscosity of the fluid, ω is the angular frequency, and the effective parameters are the complex and frequency-dependent dynamic viscous permeability tensor \mathbf{k} and compressibility C of the equivalent fluid. These suffice to describe the long-wavelength acoustic properties of rigid-frame SPM and can be calculated, for a material with known microstructure, from the solution of leading-order boundary value problems (i.e. oscillatory Stokes and heat conduction problems) arising from homogenisation [6, 10, 11, 13–17], or using either empirical models [1, 3] or models that make use of scaling functions [7, 10, 13–18]. While \mathbf{k} accounts for the acoustic losses due to gas viscosity, C does so for those due to heat exchanges between the frame and the gas. Using these effective parameters, one can calculate the effective wavenumber \mathbf{k}_c and characteristic impedance \mathbf{Z}_c as

$$\mathbf{k}_c = \omega \sqrt{\frac{\eta \mathbf{k}^{-1} C}{j\omega}}, \quad (3)$$

$$\mathbf{Z}_c = \sqrt{\frac{\eta \mathbf{k}^{-1}}{j\omega C}}. \quad (4)$$

The effective parameters \mathbf{k}_c and \mathbf{Z}_c can then be used to calculate acoustic descriptors of material layers of thickness d . For example, when placing an isotropic porous layer on a perfectly-rigid and impervious wall and the sound waves impinge perpendicularly to its surface, the surface impedance Z_w of the layer is a scalar given by

$$Z_w(\omega) = -jZ_c \cot(k_c d), \quad (5)$$

while its sound absorption coefficient $\mathcal{A}(\omega)$, which takes values between zero (perfect reflection) and one (perfect absorption), reads as

$$\mathcal{A}(\omega) = \frac{4X}{(1+X)^2 + Y^2}, \quad (6)$$

where $X = \text{Re}(Z_w)/Z_0$ is the normalised resistance and $Y = \text{Im}(Z_w)/Z_0$ is the normalised reactance. In these expressions, $Z_0 = \rho_0 c_0$ denotes the characteristic impedance of the fluid adjacent to the layer (i.e. air) and ρ_0 and c_0 are the equilibrium density of and speed of sound in air, respectively.

From Eq. (6), it is clear that \mathcal{A} is maximised when the following condition, known as impedance matching [1, 3], is satisfied

$$X = 1, \quad \text{i.e.} \quad \text{Re}(Z_w) = Z_0, \quad \text{and} \quad Y = 0. \quad (7)$$

This condition is relatively easy to achieve by conventional SPM at mid and high frequencies but very difficult to do so at low frequencies, unless one considers bulky materials, which are impractical for engineering applications where the space is limited.

Several research avenues have been explored to overcome the lack of efficiency of conventional porous materials in attenuating low-frequency sound waves. For example, low-frequency sound absorption can be improved by stacking multiple layers of permeable materials [1, 3, 19, 20]. This could be achieved by judiciously selecting the first layer (i.e. the one facing the waves) so that the real part of its surface impedance matches the characteristic impedance of air and its reactance magnitude is as small as possible, while the inner layers provide additional sound attenuation. A similar approach was taken in [21], where an impedance matching layer was used to improve the sound absorption of a porous core. Even though the staking of layers or the use of an impedance matching layer can actually lead to increase sound absorption, the overall thickness of the material could still be considerable. To tackle this issue, other types of materials, such as metamaterials [22–32] and multiscale porous materials [33–40], have been investigated. In addition to these investigations, one can mention experimental and numerical works on wave propagation in porous composites that are relevant to this paper, e.g. [41–53]. In these works, the often superior sound absorptive properties of porous composites in comparison with those of their constituents is demonstrated. However, a well established theory that rigorously captures the acoustic interaction between the porous constituents of the composite as well as thorough understanding of the physical mechanisms by which the sound attenuation by porous composites is achieved are, to our knowledge, still lacking. Such an understanding can lead to determine the conditions for which porous composites can present superior acoustic performance in comparison with that of their individual constituents, as well as to guide the rational design of optimised noise mitigation solutions.

This paper investigates acoustic wave propagation in gas-saturated rigid-frame porous composites with arbitrary but periodic microstructure. The macroscopic description of acoustic wave propagation in such composites is obtained by using the two-scale asymptotic method of homogenisation and reveals the underlying physical mechanisms of dissipation of sound energy. Through the analysis of the effective parameters and acoustic descriptors, the conditions under which porous composites can provide more efficient noise reduction than their conventional permeable constituents are determined. The developed theory is exemplified by introducing analytical models for the effective acoustical properties of porous composites with canonical inclusion patterns (i.e. a porous matrix with a periodic array of cylindrical or spherical inclusions) as well as validated by comparing the models predictions with the results of direct finite-element simulations and experimental testing. In short, the key contributions of this paper are: i) the introduction of a general homogenisation-based theory of acoustic wave propagation in rigid-frame porous composites, ii) the derivation of analytical models for the acoustic properties of porous composites with canonical microstructure, and iii) the numerical and experimental validation of the upscaled theory.

2 Sound propagation in porous composites – Theory

2.1 Geometry

Let us consider a periodic rigid-frame porous composite saturated with air. A sketch of its geometry is shown in Fig. 1. The representative elementary volume (REV) of the porous composite, denoted as Ω , comprises a connected porous matrix Ω_m that faces the incident waves and a single inclusion Ω_i . From now on, the subscripts m and i label, respectively, the porous matrix and the inclusion. The interface between the porous matrix and the inclusion is $\Gamma = \partial\Omega_m \cap \partial\Omega_i$. The volume fractions of the porous matrix and inclusion are respectively calculated as $\varphi_m = \Omega_m/\Omega$ and $\varphi_i = \Omega_i/\Omega$, while their porosities are ϕ_m and ϕ_i . Hence, the overall porosity of the porous composite is $\phi = \varphi_m\phi_m + \varphi_i\phi_i$.

The period of the material is $\ell \ll L = \lambda/2\pi$ and the existence of two distinct characteristic sizes enables to define the small parameter $\varepsilon = \ell/L \ll 1$.

2.2 Local description

The air-saturated porous constituents of the composites have a perfectly rigid and motionless solid frame. As such, only propagation of waves in the fluid saturating the porous constituents is allowed. The porous constituents, i.e. the matrix and inclusions, are modelled as equivalent Darcy media with known effective parameters. The effective parameters of the porous matrix are the dynamic viscous permeability tensor \mathbf{k}_m and effective compressibility C_m . Similarly, the effective parameters of the porous inclusions are \mathbf{k}_i and C_i and these, unless otherwise explicitly stated, satisfy the conditions $|\mathbf{k}_i| \ll |\mathbf{k}_m|$ and $|C_i| = O(|C_m|)$, i.e. the porous inclusion is much less permeable than the porous matrix, while the effective compressibilities are comparable.

Acoustic wave propagation in the porous matrix is governed by the effective equation of conservation of mass (8) and the dynamic Darcy's law (9), namely

$$\nabla \cdot \mathbf{V}_m + j\omega p_m C_m(\omega) = 0 \quad \text{in } \Omega_m, \quad (8)$$

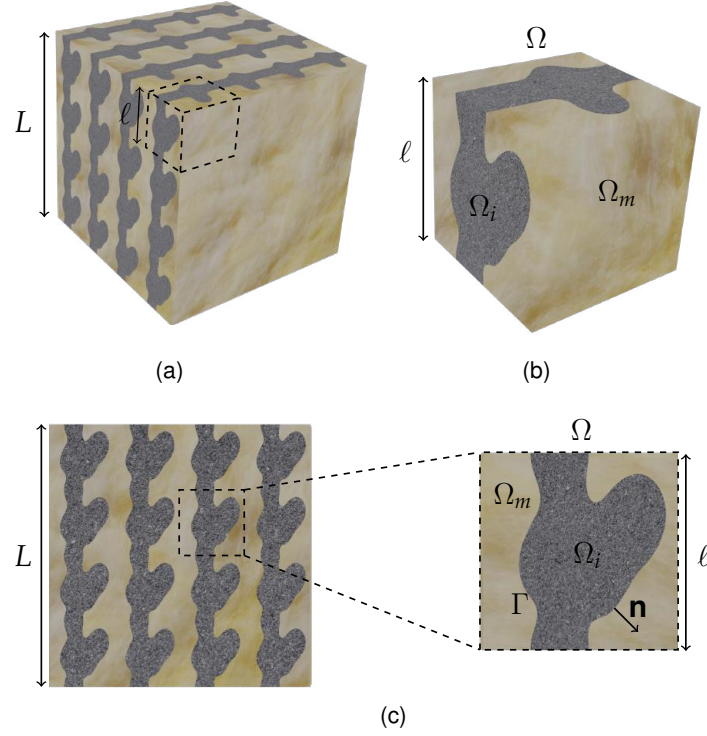


Figure 1: Sketch of the geometry of a generic porous composite (a), its 3D representative elementary volume REV (b), and a 2D representation of the REV (c).

$$\mathbf{V}_m = -\frac{\mathbf{k}_m(\omega)}{\eta} \cdot \nabla p_m \quad \text{in } \Omega_m, \quad (9)$$

where \mathbf{V}_m and p_m are the Darcy velocity and pressure in the porous matrix, respectively. Note that harmonic dependence of the type $e^{j\omega t}$ is adopted and, for the sake of simplicity, this term is omitted throughout the paper.

Similarly, the propagation of acoustic waves in the porous inclusions is governed by the effective equation of conservation of mass (10) and the dynamic Darcy's law (11), namely

$$\nabla \cdot \mathbf{V}_i + j\omega p_i C_i(\omega) = 0 \quad \text{in } \Omega_i, \quad (10)$$

$$\mathbf{V}_i = -\frac{\mathbf{k}_i(\omega)}{\eta} \cdot \nabla p_i \quad \text{in } \Omega_i, \quad (11)$$

where \mathbf{V}_i and p_i are the Darcy velocity and pressure in the porous inclusion, respectively.

The Eqs. (8)-(11) are coupled via boundary conditions which represent the continuity of normal velocity (12) and of pressure (13), i.e. (with \mathbf{n} being a unit normal vector, see Fig. 1c)

$$\mathbf{V}_m \cdot \mathbf{n} = \mathbf{V}_i \cdot \mathbf{n} \quad \text{on } \Gamma, \quad (12)$$

$$p_m = p_i \quad \text{on } \Gamma. \quad (13)$$

The set of equations (8)-(13) is upscaled using the two-scale asymptotic homogenisation method (see Appendix A). The general steps of the method are: the rescaling of the local description based on a physical analysis, the formulation of the unknown variables as series expansion in terms of the small parameter ε , the identification of leading-order boundary value problems, and the derivation of the macroscopic effective equations. This final result is presented in the next subsection. Note also that the homogenisation procedure provides the recipe to calculate the effective parameters of the porous composite modelled as an equivalent fluid.

2.3 Macroscopic description

The derivation of the macroscopic equations that describe acoustic wave propagation in porous composites with highly contrasted permeabilities is detailed in Appendix A. These equations correspond to the macroscopic mass balance equation (14) and the dynamic Darcy's law written further below. With $\mathbf{V}_m^{(0)}$ and $p_m^{(0)}$ being the leading-order Darcy velocity and pressure, the former reads as

$$\nabla_x \cdot \langle \mathbf{V}_m^{(0)} \rangle + j\omega p_m^{(0)} C(\omega) = 0. \quad (14)$$

This equation takes the same mathematical form as the macroscopic mass balance equation for single porosity materials [see Eq. (1)]. However, the effective compressibility is rather different and given by

$$C(\omega) = \varphi_m C_m(\omega) + \varphi_i C_i(\omega) \mathcal{F}(\omega). \quad (15)$$

Here, it is recalled that φ_m and φ_i are the volume fractions of the porous matrix and inclusions, respectively; while C_m and C_i are the effective compressibilities of the porous constituents. The function \mathcal{F} is given by

$$\mathcal{F}(\omega) = 1 - \frac{j\omega B(\omega)}{\varphi_i \mathcal{D}(\omega)}, \quad (16)$$

where, for isotropic inclusions, the pressure diffusivity, given by $\mathcal{D}(\omega) = \mathcal{K}_i / \eta C_i$, depends on the dynamic viscous permeability \mathcal{K}_i and effective compressibility C_i of the porous inclusion. The pressure diffusion function $B(\omega)$ is calculated as

$$B(\omega) = \frac{1}{\Omega} \int_{\Omega_i} \bar{b}(y, \omega) d\Omega, \quad (17)$$

where $\bar{b}(y, \omega)$ is determined from the solution of Eqs. (A.18)–(A.19), as discussed in Appendix A.

The dynamic Darcy's law of the porous composite also takes the same mathematical form as that for single porosity materials [see Eq. (2)], i.e.

$$\langle \mathbf{V}_m^{(0)} \rangle = -\frac{\mathbf{k}(\omega)}{\eta} \cdot \nabla_x p_m^{(0)}. \quad (18)$$

However, the dynamic viscous permeability tensor $\mathbf{k}(\omega)$ is given by

$$\mathbf{k} = \varphi_m \mathbf{k}_m \cdot \boldsymbol{\alpha}_\infty^{-1}. \quad (19)$$

where $\boldsymbol{\alpha}_\infty$ is a tortuosity tensor induced by the presence of the inclusions (see Appendix A).

The macroscopic wave equation is then obtained by eliminating the Darcy velocity in Eq. (14). From the resulting equation, it is direct to derive the expressions for the wave number and characteristic impedance given by Eqs. (3) and (4), respectively. However, the effective parameters \mathbf{k} and C are now calculated from Eqs. (19) and (15). Note that this is also the case for porous composites with perfectly impervious inclusions; nonetheless, for this case $C_i = 0$ and, therefore, the effective compressibility is calculated as

$$C(\omega) = \varphi_m C_m(\omega). \quad (20)$$

For the sake of completeness, the expressions for the effective compressibilities of the porous constituents are calculated as [10]

$$C_u(\omega) = \frac{\phi_u}{P_0} \left(1 - \frac{\gamma - 1}{\gamma} \frac{j\omega}{\omega_{tu}} \frac{\Theta_u(\omega)}{\Theta_{0u}} \right) \quad \text{with } u = m, i, \quad (21)$$

where $\Theta_u(\omega)$ are the thermal permeabilities, $\Theta_{0u} = \Theta_u(\omega = 0)$ are the static thermal permeabilities, $\omega_{tu} = \phi_u \frac{\alpha}{\Theta_{0u}}$ are the thermal characteristic frequencies, and ϕ_u are the porosities of the porous matrix ($u = m$) and porous inclusions ($u = i$). The physical parameters are the equilibrium pressure P_0 and the specific heat ratio γ and thermal diffusivity α of the saturating fluid.

To summarise, the introduced macroscopic description of acoustic wave propagation in rigid-frame porous composites, given by Eqs. (14) and (18), reveals that the dynamic viscous permeability [see Eq. (19)] is modified by the presence of the porous inclusions. In comparison with the dynamic viscous permeability of a single porosity material made from the porous matrix material, \mathbf{k} is reduced by both the tortuosity effect induced by the inclusions and the volume fraction of the porous matrix. On the other hand, the effective compressibility [see Eq. (15)], similarly to double [34–37] or multiple porosity [38–40] media, becomes significantly modified by the pressure diffusion phenomenon, characterised by $B(\omega)$, which induces additional and tunable sound energy dissipation.

At this point, it is pertinent to point out that the macroscopic equations that describe acoustic wave propagation in rigid-frame porous composites whose constituents have comparable permeabilities and compressibilities, i.e. $|\mathbf{k}_i| = O(|\mathbf{k}_m|)$ and $|C_i| = O(|C_m|)$, take the same mathematical form as Eqs. (14) and (18). However, as derived in Appendix B, the effective compressibility and dynamic viscous permeability tensor are given by

$$C(\omega) = \varphi_m C_m(\omega) + \varphi_i C_i(\omega), \quad (22)$$

$$\mathbf{k} = \varphi_m \mathbf{k}_m \cdot \boldsymbol{\Xi}_m + \varphi_i \mathbf{k}_i \cdot \boldsymbol{\Xi}_i, \quad (23)$$

where $\boldsymbol{\Xi}_m$ and $\boldsymbol{\Xi}_i$, defined in Eq. (B.3), are, in general, complex-valued frequency-dependent tensors that also depend on the geometry of the composite. However, for composites with inclusions having constant cross-section and sound propagation in the direction along the inclusions axis, the said tensors become the identity tensors, i.e. $\boldsymbol{\Xi}_m = \boldsymbol{\Xi}_i = \mathbf{I}$. Moreover, Eqs. (22) and (23) allow to conclude that the dissipation of sound energy in composites with weakly contrasted permeabilities is due to the combination of classical visco-thermal dissipation mechanisms in the matrix and inclusion.

2.4 Analysis of the acoustic properties

This section analyses the low-frequency asymptotic behaviour of the effective parameters of porous composites and the acoustic descriptors of porous composite layers. For simplicity, the analysis is conducted for macroscopically isotropic porous composites. This means that we will consider that $\mathbf{k} = \mathcal{K}\mathbf{I}$, $\mathbf{k}_m = \mathcal{K}_m\mathbf{I}$, $\mathbf{k}_i = \mathcal{K}_i\mathbf{I}$, and $\alpha_\infty = \alpha_\infty\mathbf{I}$. It should however be stressed that the identified generic features hold for anisotropic porous composites when considering a preferential flow direction. Moreover, the analysis will be conducted for composites for which the matrix is much more permeable than the inclusions. For the opposite case, and provided that the most permeable constituent faces the sound waves, the results hold by swapping the subscripts m and i .

Following [7], the dynamic viscous permeability of the porous matrix tends to $\mathcal{K}_m(\omega \ll \omega_{vm}) = \mathcal{K}_{0m}$, where \mathcal{K}_{0m} , $\omega_{vm} = \phi_m\nu/\mathcal{K}_{0m}\alpha_{\infty m}$ and $\alpha_{\infty m}$ are, respectively, the static viscous permeability, viscous characteristic frequency, and tortuosity of the porous matrix material, while $\nu = \eta/\rho_0$ is the kinematic viscosity of air. The limiting value of the dynamic viscous permeability of the porous composite, in the quoted frequency range, is therefore given by

$$\mathcal{K}(\omega \ll \omega_{vm}) \approx \frac{\phi_m}{\alpha_\infty} \mathcal{K}_{0m} = \mathcal{K}_0. \quad (24)$$

From this equation, it is clear that the static viscous permeability of the porous composite \mathcal{K}_0 is smaller than that of the material the porous matrix is made from. In other words, the static viscous permeability of the porous matrix material is reduced by a factor of $(1 - \varphi_i)/\alpha_\infty$ due to the presence of the weakly permeable inclusions.

The low-frequency behaviour of the effective compressibilities $C_u(\omega)$ (with $u = m, i$) is characterised by that of the dynamic thermal permeabilities Θ_u . For $\omega \ll \omega_{tu}$, Θ_u tends to $\Theta_{0u} = \Theta_u(\omega = 0)$. Hence, one has that

$$C_u(\omega \ll \omega_{tu}) \approx \frac{\phi_u}{P_0} \left(1 - \frac{\gamma - 1}{\gamma} \frac{j\omega}{\omega_{tu}} \right) \quad \text{i.e.} \quad C_{0u} = C_u(\omega = 0) = \frac{\phi_u}{P_0}. \quad (25)$$

Since $B(\omega)$ varies [33, 34] from $B(\omega \ll \omega_b) \approx B_0 = B(\omega = 0)$ to $B(\omega \gg \omega_b) \approx -j\varphi_i\delta_b^2$, where $\omega_b = \varphi_i\mathcal{D}_0/B_0$ is the pressure diffusion characteristic frequency, $\delta_b = \sqrt{\mathcal{D}_0/\omega}$ is the pressure diffusion boundary layer thickness, and $\mathcal{D}_0 = \mathcal{K}_{0i}P_0/\eta\phi_i$ is the static pressure diffusivity, the function \mathcal{F} takes the following asymptotic values

$$\mathcal{F}(\omega \ll \omega_b) \approx 1 - \frac{j\omega}{\omega_b}, \quad \mathcal{F}(\omega \gg \omega_b) \approx 0. \quad (26)$$

The latter equation shows that the influence of the porous inclusions on the effective compressibility vanishes for frequencies much higher than the pressure diffusion characteristic frequency. In other words, for $\omega \gg \omega_b$, the weakly permeable inclusions acoustically behave as if they were perfectly impervious.

By inserting Eqs. (25) and (26) into Eq. (15) and retaining only linear terms in frequency, one obtains that the effective compressibility of the porous composites exhibits the following low-frequency asymptotic behaviour

$$C_{\text{If}} = C(\omega \ll \min(\omega_{tp}, \omega_b, \omega_{ti})) \approx \frac{1}{P_0} \left(\phi - \frac{j\omega}{\omega_g} \right), \quad (27)$$

where ω_g is a characteristic frequency of the porous composite defined by

$$\frac{1}{\omega_g} = \frac{\gamma - 1}{\gamma} \frac{\varphi_m\phi_m}{\omega_{tm}} + \varphi_i\phi_i \left(\frac{\gamma - 1}{\gamma} \frac{1}{\omega_{ti}} + \frac{1}{\omega_b} \right). \quad (28)$$

Then, the static effective compressibility of the porous composite is given by

$$C_0 = \frac{\phi}{P_0}. \quad (29)$$

Using the asymptotic low-frequency values for $C(\omega)$ and $\mathcal{K}(\omega)$, the following limiting values for the wave number k_c , effective speed of sound $c_e = \omega/k_c$, and characteristic impedance Z_c are derived (with $\Phi = 1 + \frac{\varphi_i\phi_i}{\varphi_m\phi_m} \geq 1$)

$$\frac{k_c(\omega \rightarrow 0)}{k_{cm}(\omega \rightarrow 0)} = \sqrt{\alpha_\infty\Phi} \quad \text{with} \quad k_{cm}(\omega \rightarrow 0) = \omega \sqrt{\frac{\eta}{j\omega\mathcal{K}_{0m}P_0}}, \quad (30)$$

$$\frac{c_e(\omega \rightarrow 0)}{c_{em}(\omega \rightarrow 0)} = \frac{1}{\sqrt{\alpha_\infty\Phi}} \quad \text{with} \quad c_{em}(\omega \rightarrow 0) = \frac{\omega}{k_{cm}(\omega \rightarrow 0)}, \quad (31)$$

$$\frac{Z_c(\omega \rightarrow 0)}{Z_{cm}(\omega \rightarrow 0)} = \frac{1}{\varphi_m} \sqrt{\frac{\alpha_\infty}{\Phi}} \quad \text{with} \quad Z_{cm}(\omega \rightarrow 0) = \sqrt{\frac{\eta P_0}{j\omega\mathcal{K}_{0m}\phi_m}}. \quad (32)$$

In comparison with the wave number of the porous matrix material (subscript m), the wave number of the porous composite is increased, as shown in Eq. (30), by a factor of $\sqrt{\alpha_\infty \tilde{\Phi}}$. Recalling that the attenuation coefficient is defined as $A_t = -\text{Im}(k_c)$, it is concluded that in the frequency range where the approximations made in the analysis are valid, i.e. for $\omega \ll \omega_{\min}$ with $\omega_{\min} = \min(\omega_{tm}, \omega_{ti}, \omega_{vm}, \omega_{vi}, \omega_b)$, the sound attenuation by the highly permeable matrix is increased when adding much less permeable inclusions to it. On the other hand, Eq. (31) shows that the effective speed of sound in the porous composite is slowed down in the presence of the inclusions. Moreover, Eq. (32) reveals that the characteristic impedance of the porous composite is larger than that of the porous matrix material.

To gain insight into the acoustic behaviour of a hard-backed porous composite layer of thickness d , its surface impedance is approximated, for the case $|k_c d| \ll 1$ and $\omega \ll \omega_{\min}$, by expanding Eq. (5) to obtain $Z_w/Z_0 = X + jY$, where the normalised resistance X and reactance Y are given by

$$X \approx \frac{\eta}{\mathcal{K}_0} \frac{d}{3Z_0} = X_m \frac{d}{d_m} \frac{\alpha_\infty}{\varphi_m} \quad \text{with} \quad X_m = \frac{\eta}{\mathcal{K}_{0m}} \frac{d_m}{3Z_0}, \quad (33)$$

$$Y \approx -\frac{P_0}{\omega \phi d Z_0} = Y_m \frac{\phi_m}{\phi} \frac{d_m}{d} \quad \text{with} \quad Y_m = -\frac{P_0}{\omega \phi_m d_m Z_0}. \quad (34)$$

Eq. (33) indicates that for a porous composite with the same thickness of a hypothetical porous layer made from the porous matrix material with thickness $d_m = d$, its normalised resistance is α_∞/φ_m times larger. Recalling that one of the requirements to fully satisfy the impedance matching condition is $X = 1$, one has that if $X_m < 1$, then adding inclusions to the porous matrix appears as a practical way of matching the real part of the surface impedance with the characteristic impedance of air, which in turn can lead to maximising the sound absorption coefficient \mathcal{A} , defined in Eq. (6). Indeed, a simple expression that can guide the optimisation of the sound absorptive behaviour of a porous composite is $\alpha_\infty d/\varphi_m d_m = 1/X_m$ or, equivalently, $\alpha_\infty d/\varphi_m = 3Z_0/\sigma_{0m}$, where $\sigma_{0m} = \eta/\mathcal{K}_{0m}$ is the static flow resistivity of the porous matrix material. Since the tortuosity α_∞ , as will be shown below, depends mainly on the volume fraction of the porous matrix φ_m , it is remarkable that only φ_m and d are required to induce the impedance matching. On the other hand, if $X_m > 1$, then the sound absorption coefficient of the porous composite is expected to take smaller values in comparison with that of the porous matrix without inclusions but the same thickness.

Regarding the normalised reactance and for $d_m = d$, Eq. (34) shows that its magnitude increases, which is detrimental to maximising low-frequency sound absorption, unless $\phi > \phi_m$ which is obtained for $\phi_i > \phi_m$. The latter inequality is certainly possible but might not contribute to satisfy a key condition, i.e. $\mathcal{K}_i \ll \mathcal{K}_m$, the developed theory is based on. On the other hand, it is recalled that the approximations made so far in the analysis are restricted to $\omega \ll \omega_{\min}$ and $|k_c d| \ll 1$. A more general case is one in which the effective parameters cannot be approximated by simple expressions. It is however possible to determine for materials with real-valued characteristic impedance and wave number, which is approximately the case when sound propagation is dominated by the inertia of the effective fluid, that the first peak in the absorption coefficient appears when the cotangent in Eq. (5) is zero. This occurs when $\text{Re}(k_c) = \pi/2d$ or, in terms of the ratio between the layer thickness and the effective wavelength $\lambda_c = 2\pi/k_c$, when $\text{Re}(d/\lambda_c) = 1/4$. This is usually known as the quarter-wavelength 'rule'. It shows that the first peak of absorption occurs at a frequency, say f_0 , for which the layer thickness is a quarter of the sound wavelength. Since low-frequency sound waves have long wavelengths, thick materials are generally required to absorb them efficiently.

Using Eqs. (3), (15) and (19), it is direct to show that, for all frequencies, the effective wavelength in the porous matrix material, i.e. $\lambda_m = 2\pi/k_{cm}$, is longer than that in a porous composite λ_c . Specifically, one has that $\lambda_m/\lambda_c = \sqrt{\alpha_\infty \tilde{\Phi}}$. Note that $\tilde{\Phi} = 1$ for a composite with impervious inclusions. For a composite with porous inclusions one has that $\tilde{\Phi} = 1 + \varphi_i C_i \mathcal{F}/\varphi_m C_m$, which equals to $\tilde{\Phi} = 1 + \frac{\varphi_i \phi_i}{\varphi_m \phi_m}$ when $\omega \ll \omega_{\min}$ while it takes its maximum value when: i) $\mathcal{F}(\omega \ll \omega_b) = 1$, ii) the effective compressibility of the porous inclusion takes its isothermal value, i.e. $C_i(\omega \ll \omega_{ti}) = \phi_i/P_0$, and iii) the effective compressibility of the porous matrix takes its adiabatic value, i.e. $C_m(\omega \gg \omega_{tm}) = \phi_m/\gamma P_0$. Under these conditions, which favour the difference in effective wavelengths, one has that $\tilde{\Phi} = 1 + \gamma \varphi_i \phi_i/\varphi_m \phi_m$.

The analysis for both types of porous composites leads to the conclusion that the first absorption peak of a porous composite layer is usually located at a lower frequency than that of a layer made solely from the porous matrix material since for composites $Y \rightarrow 0$ at a lower frequency. This condition, together with ensuring that $X \rightarrow 1$ which can be achieved by tuning the layer thickness and φ_m as discussed above, yields a simple design criterion for improving the sound absorption properties of a highly permeable matrix by adding weakly permeable or impervious inclusions to it.

To finalise this section, let us remark that the analysis of the acoustic properties of composites with weakly contrasted permeabilities is similar. Specifically, for frequencies much smaller than either the viscous or thermal characteristic frequencies of the constituents, the dynamic permeability tends to $\mathcal{K}_0 = \varphi_m \mathcal{K}_{0m} \Xi_{0m} + \varphi_i \mathcal{K}_{0i} \Xi_{0i}$, where Ξ_{0m} and Ξ_{0i} are defined by Eq. (B.3) (for $\omega = 0$), while the compressibility tends to its static value given by Eq. (29). Then, the low-frequency asymptotic values of the effective wave number, speed of sound, and characteristic impedance are obtained by making the replacement $\alpha_\infty \rightarrow \Xi_{0m}^{-1}(1 + \varphi_i \mathcal{K}_{0i} \Xi_{0i}/\varphi_m \mathcal{K}_{0m} \Xi_{0m})^{-1}$ in Eqs. (30)–(32). As discussed at the end of §2.3, $\Xi_{0m} = \Xi_{0i} = 1$ for composites with inclusions having constant cross-section and sound propagation in the direction along the inclusions axis. Hence, for such composites, and provided that $\mathcal{K}_{0i}/\varphi_i \leq \mathcal{K}_{0m}/\varphi_m$, it results that the analysis of the surface impedance [see Eq. (33)–(34) and related discussion] holds. In addition, similar results are obtained when

the quoted inequality is reversed but the subscripts m and i shall be adequately swapped in the numbered expressions of this section.

2.5 Analytical models

To exemplify the developed theory, analytical models for porous composites with i) cylindrical and ii) spherical inclusions are introduced. The geometry for both types of porous composites is depicted in Fig. 2. The porous matrix and porous inclusions are assumed as made from a fibrous material with regularly-arranged cylindrical fibres [54] and a granular material [55, 56], respectively. For the sake of brevity, their effective parameters, namely \mathcal{K}_m , C_m , \mathcal{K}_i , and C_i , are calculated with models that rely on scaling functions, as detailed in Appendix C.

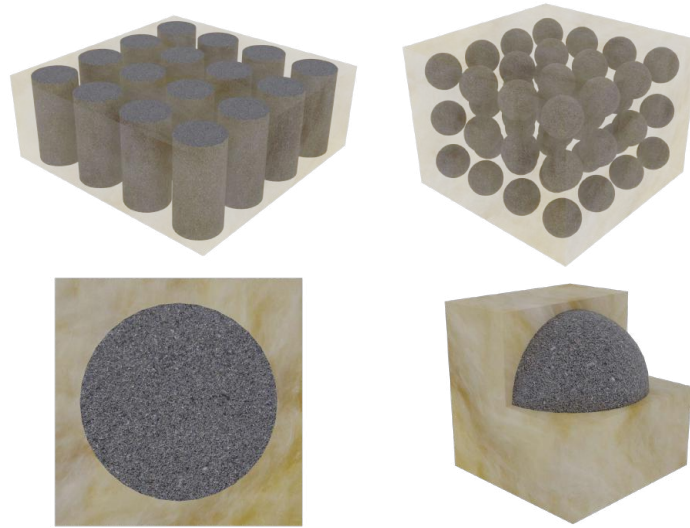


Figure 2: Illustrations of the 3D geometry (top) and unit cell (bottom) of an air-saturated porous composite with cylindrical (left) and spherical (right) inclusions. For the latter, the 3D unit cell is cut off to make the inclusion visible.

2.6 Porous composites with cylindrical inclusions

For porous composites having cylindrical porous inclusions, with radius r_i , arranged in a square lattice, sound propagation in the direction perpendicular to the inclusions axes is considered. The unit cell of the composite is a square with area b^2 . Hence, the volume fraction occupied by the porous matrix is $\varphi_m = 1 - \pi r_i^2/b^2$, while that of the porous cylindrical inclusions is $\varphi_i = 1 - \varphi_m$. The dynamic viscous permeability of the composite is calculated using Eq. (19) and is given by (see [54] for the derivation of α_∞)

$$\mathcal{K}(\omega) = \frac{\varphi_m \mathcal{K}_m(\omega)}{\alpha_\infty} = \frac{\varphi_m \mathcal{K}_m(\omega)}{2 - \varphi_m}. \quad (35)$$

The effective compressibility of the porous composite with cylindrical porous inclusions is calculated from Eq. (15). This requires knowing C_m and C_i (see Appendix C for their expressions) and \mathcal{F} which depends on B . For the latter, a model has been derived in [37] by noting that the pressure diffusion boundary-value problem [Eqs. (A.18)–(A.19)] formulated in a porous cylindrical inclusion is formally identical to an oscillatory fluid flow or heat conduction problem formulated in a cylindrical pore. Hence, the pressure diffusion function reads as

$$B(\omega) = -j\varphi_i \delta_d^2 \left(1 - \frac{2 J_1(\xi)}{\xi J_0(\xi)} \right), \quad (36)$$

where $\xi = j^{3/2} r_i \delta_d^{-1}$, $\delta_d = \sqrt{\mathcal{D}/\omega}$, $\mathcal{D} = \mathcal{K}_i/\eta C_i$, and J_0 and J_1 are Bessel functions of the first kind of order 0 and 1, respectively. Note also that the static value of B for the porous composite with cylindrical porous inclusions is $B_0 = \varphi_i r_i^2/8$.

It must be recalled that the expressions (35)–(36) are valid for composites for which the porous matrix is much more permeable than the porous inclusions. The situation where the porous matrix is much less permeable than the cylindrical porous inclusions can be dealt with, for the case of sound propagation parallel to the inclusion axis, as follows. The dynamic viscous permeability is given by Eq. (35) with the subscript m replaced by i and noting that for this case $\alpha_\infty = 1$ (see [54]). The effective compressibility is given by Eq. (15) with the subscripts m and i being swapped. The function \mathcal{F} depends on B , which can be calculated by using the equation 66 in [39].

For porous composites with cylindrical impervious inclusions, the dynamic viscous permeability is given by Eq. (35) (with $\alpha_\infty = 2 - \varphi_m$ for perpendicular and $\alpha_\infty = 1$ for parallel wave propagation with respect the inclusion axis), while the effective compressibility is given by Eq. (20).

2.7 Porous composites with spherical inclusions

For porous composites having spherical inclusions with radius r_i and a cubic unit cell with size b , the volume fraction of the porous matrix is $\varphi_m = 1 - 4\pi r_i^3/3b^3$, while that of the spherical inclusions is $\varphi_i = 1 - \varphi_m$. The dynamic viscous permeability of the composite is calculated using Eq. (19) and is given by (see [55] for the derivation of α_∞)

$$\mathcal{K}(\omega) = \frac{2\varphi_m \mathcal{K}_m(\omega)}{3 - \varphi_m}. \quad (37)$$

The effective compressibility of the porous composite with spherical porous inclusions is calculated by using Eq. (15). This requires knowing C_m and C_i (see Appendix C), and also \mathcal{F} which depends on B . The latter has been derived in [35] and is given by

$$B(\omega) = -j\varphi_i \delta_d^2 \left(1 - \frac{3}{\xi^2} (1 - \xi \cot(\xi)) \right), \quad (38)$$

where $\xi = j^{3/2} \frac{r_i}{\delta_d}$, $\delta_d = \sqrt{\mathcal{D}/\omega}$, $\mathcal{D} = \mathcal{K}_i/\eta C_i$. Note also that $B_0 = \varphi_i r_i^2/15$.

For porous composites with spherical impervious inclusions, the dynamic viscous permeability and effective compressibility are given by Eqs. (37) and (20), respectively.

3 Illustrative examples and validation

3.1 Effective parameters

Figure 3 shows the normalised dynamic viscous permeability of a porous composite with cylindrical porous inclusions in comparison with that of the porous matrix material. The normalisation is made with respect to the static viscous permeability of the porous matrix material (i.e. \mathcal{K}_{0m}). The porous composite comprises a matrix and inclusions made from fibrous and granular materials, respectively. The microstructural parameters (see Appendix C) of these constituent materials are set to typical values, i.e. $a_m = 28 \mu\text{m}$, $\phi_m = 0.96$, $a_i = 28 \mu\text{m}$, and $\phi_i = 0.32$. Moreover, these values ensure the separation of scales required in the developed theory. The geometrical parameters of the composite are $r_i = 2 \text{ mm}$ and $b = 5.5 \text{ mm}$, which lead to $\varphi_m = 0.5846$ and $\varphi_i = 0.4154$. Sound propagation perpendicular to the inclusions axis is considered. Normal pressure ($P_0 = 101325 \text{ Pa}$) and temperature ($\tau_0 = 293.15 \text{ K}$) conditions are set here and in what follows. The plot shows that the dynamic viscous permeability of the porous matrix is reduced in presence of the porous inclusions. The viscous characteristic frequency, which denotes the transition from viscosity- to inertia-dominated flow, remains unchanged, as it is evidenced by the peaks of the imaginary parts, both located at the same frequency. Thus, the dynamic viscous permeability is scaled in amplitude but not in frequency. Note also that if the inclusions were

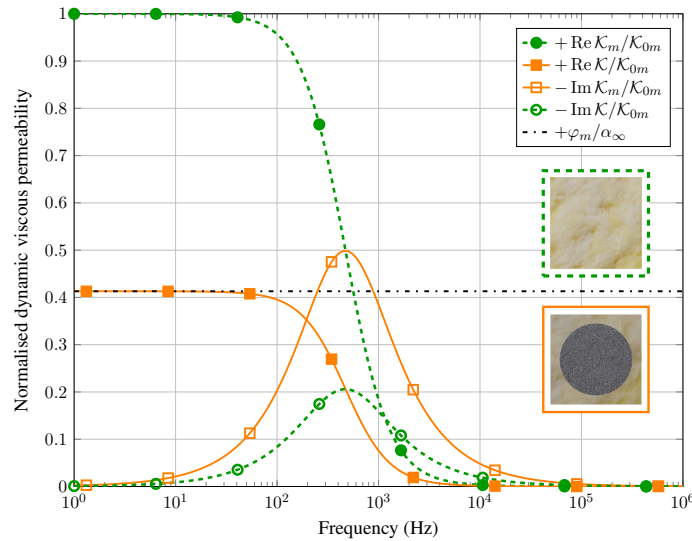


Figure 3: Real part and negative of the imaginary part of the normalised dynamic viscous permeability of the porous matrix material (dashed lines) and of the porous composite (solid lines).

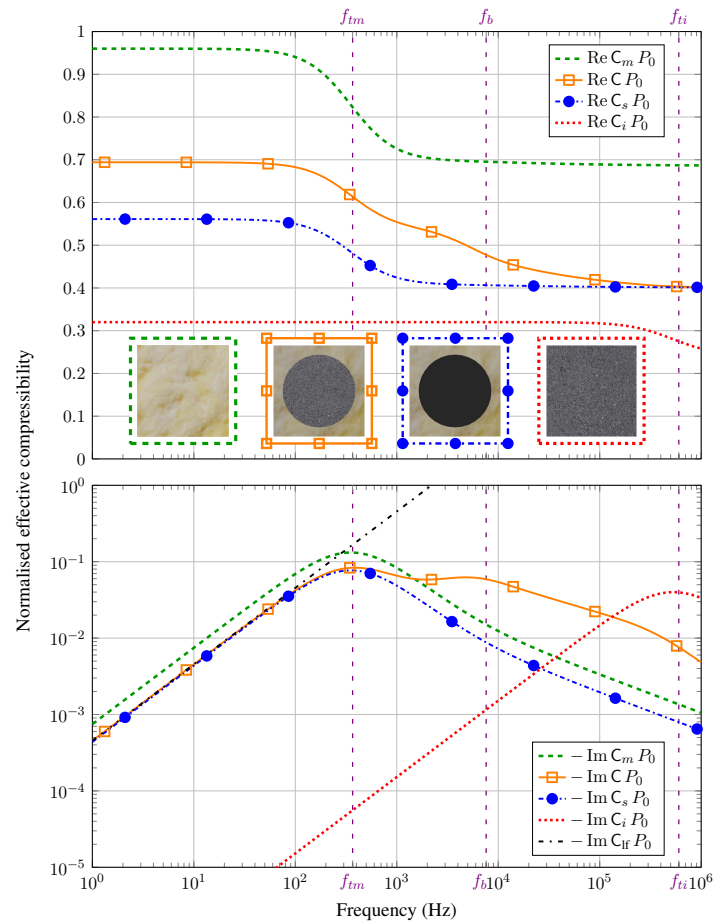


Figure 4: Real part (top) and negative of the imaginary part (bottom) of the normalised effective compressibility of the porous matrix material (subscript m), porous inclusion material (subscript i), and the corresponding porous composite with porous or solid (subscript s) impervious inclusions. The vertical dashed lines denote characteristic frequencies while the dashed dotted line represents the asymptotic value of the negative of the imaginary part of the normalised effective compressibility of the porous composite [see Eq. (27)].

perfectly impervious, the dynamic viscous permeability coincides with that of the composite with resistive inclusions. For the sake of clarity, this is not shown in the plot.

Figure 4 shows the normalised effective compressibility of the porous composite with porous cylindrical inclusions compared with the normalised effective compressibility of the porous matrix material, the porous inclusion material, and the composite with impervious inclusions. The isothermal compressibility of air $1/P_0$ is used to normalise the effective compressibilities. Focusing the discussion on the key trends, the plot shows the monotonically decreasing nature of the real part of the effective compressibility that is also characterised by transitions determined by the characteristic frequencies ω_{tm} and ω_b . Moreover, as expected from the analysis presented in §2.4, the normalised effective compressibilities of the porous composites and both constituents tend to their respective porosities at low frequencies. Hence, the normalised effective compressibility tends to ϕ or $\varphi_m \phi_m$ in the case of porous or impervious inclusions, respectively. At high frequencies, the effective compressibility of both types of composites tends to the same value. This is because $\mathcal{F} \rightarrow 0$ when $\omega \gg \omega_b$, which means that the porous inclusions behave as impervious ones for frequencies much higher than the pressure diffusion characteristic frequency. This highlights the crucial role of ω_b on the acoustic behaviour of porous composite with highly contrasted permeabilities. Indeed, it is around this frequency that the sound energy dissipation is significantly increased, as shown in Fig. 4 where a local maximum of $-\text{Im}(C)$ around ω_b can be seen. Such a feature is shared by classical double porosity media [34, 35]. In addition, it is also shown that the low-frequency asymptotic behaviour of the imaginary part of the effective compressibility is well predicted by Eq. (27).

The model introduced in §2.7 for porous composites with spherical inclusions is now used to exemplify the behaviour of the normalised attenuation coefficient and effective speed of sound of such composites. The geometrical parameters of the composite are: $r_i = 5$ mm and $b = 11$ mm, which lead to $\varphi_m = 0.6066$ and $\varphi_i = 0.3934$. The porous matrix and inclusions are made from fibrous and granular materials having the same parameters as above, i.e. $a_m = 28$ μm , $\phi_m = 0.96$, $a_i = 28$ μm , and $\phi_i = 0.32$.

Figure 5 shows that the normalised attenuation coefficient of the porous composite with spherical porous inclusions is higher than that of the porous composite with impervious inclusions. This confirms the analysis of the effective properties presented in §2.4 and highlights the effect of the pressure diffusion phenomenon on the sound attenuating behaviour of a permeable matrix with porous inclusions. As expected, the effective speed of sound in the composite with porous

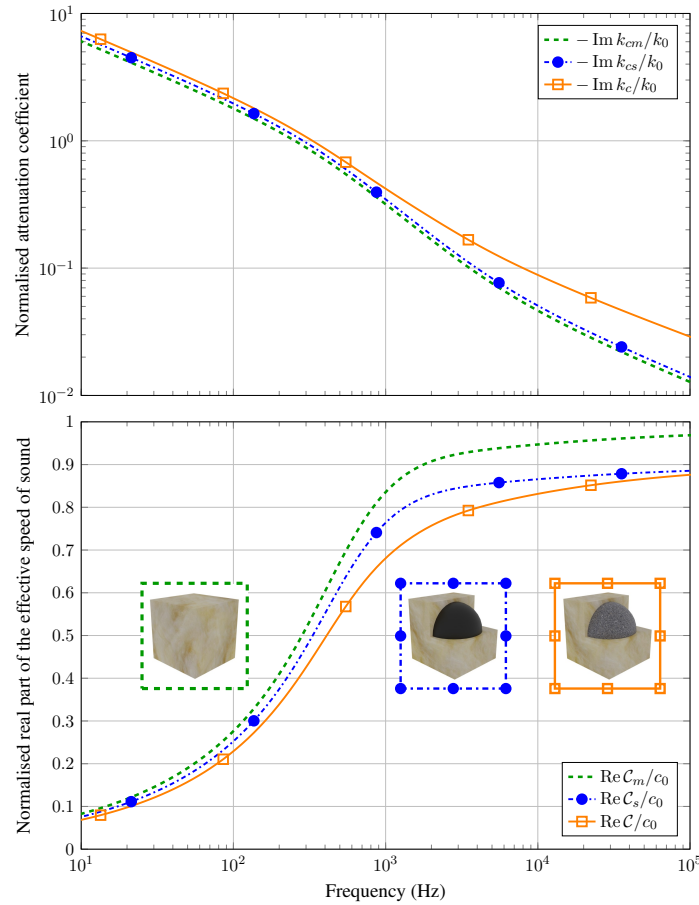


Figure 5: Normalised attenuation coefficient (top) and real part of the speed of sound (bottom) as a function of frequency for a porous composite with porous (solid line) or solid impervious (dash-dotted line) spherical inclusions and the porous matrix material (dashed line).

inclusions is slower, in the whole frequency range, than that in the same composite but with impervious inclusions, as also shown in Fig. 5. In addition, the presented results also confirm that by adding inclusions to the porous matrix an increase (respectively, decrease) in normalised attenuation coefficient (respectively, effective speed of sound) is achieved.

To conclude, the results presented in this section show that both effective parameters, i.e. the dynamic viscous permeability and effective compressibility, contribute to explain the improvement in intrinsic acoustic performance of the composite over that of the highly permeable matrix material alone. Such an improvement, evidenced by the higher attenuation coefficient of the composite (see Fig. 5), is determined, on the one hand, by the reduction of the matrix volume fraction due to the presence of the weakly permeable or impervious inclusions as well the tortuosity effect such inclusions induce; and, on the other hand, by the additional sound energy dissipation caused by the pressure diffusion phenomenon, particularly around the associated characteristic frequency ω_b (see, e.g., the bottom plot in Fig. 4), that strongly determines the effective compressibility of composites with weakly permeable inclusions. The two main effects, i.e. tortuosity and pressure diffusion, will also influence the acoustic descriptors of rigidly-backed composite layers, as will be discussed in the next subsection where the upscaled theory is also numerically validated.

3.2 Numerical validation and further discussion

To validate the developed homogenisation-based theory, analytical and direct numerical calculations of the surface impedance Z_w and sound absorption coefficient \mathcal{A} of rigidly-backed layers of porous composites with cylindrical or spherical inclusions are compared.

The surface impedance is determined analytically using Eq. (5), in which the effective wave number k_c and characteristic impedance Z_c are determined thanks to the dynamic viscous permeability and effective compressibility analytically calculated for a homogenised porous composite, as described in § 2 in general, and in subsections 2.5–2.7, and 3.1 for the particular cases of porous composites with periodically embedded cylindrical or spherical inclusions.

In the direct numerical approach, the local equations that govern the propagation of acoustic waves in the porous composite, i.e. Eqs. (8)–(13), are solved using the finite element method. That is, the Helmholtz equation for linear acoustics is formulated in each constituent of the composite. Note that the Helmholtz equation formulated in the porous matrix is obtained by combining Eqs. (8) and (9), while the one for the inclusions is obtained by combining Eqs. (10) and (11). The effective wave numbers are calculated for both porous media (i.e. the fibrous material of the matrix and the

granular material of the inclusions) using the same models that were used in the analytical calculations (see Appendix C). The microstructural parameters of the porous constituents are as in the previous sections.

To efficiently simulate the propagation of acoustic waves in the porous composites, the symmetry of their geometry is exploited in the numerical model by only considering a fragment of the porous composite geometry. Consequently, symmetry boundary conditions are applied on the symmetry boundaries of each porous composite. It should be noted that these conditions mean that the velocity normal to the symmetry plane is zero. From a mathematical point of view, these conditions require that the normal pressure gradient is set to zero at the respective boundaries, i.e. homogeneous Neumann conditions for the Helmholtz equation are set.

For the case of composites with porous inclusions, the continuity of normal velocity (12) and of pressure (13) is set on the interfaces between the matrix and the porous inclusions, while in the case of impervious inclusions, the rigid impermeable (i.e. homogeneous Neumann) boundary condition is applied on the inclusion surfaces. Note that the pressure gradient and the dynamic viscous permeabilities of both porous media are involved in the velocity continuity condition, which can be seen after inserting Eqs. (9) and (11) into the interface condition.

In each numerical validation example, the back face of the composite layer of thickness d is mounted on a rigid impermeable wall, while the front face is subjected to a unitary acoustic pressure. Note that $Z_w(\omega)$ is numerically calculated from the ratio between the acoustic pressure and the normal velocity spatially averaged on the front face of the porous composite layer. This is then inserted into Eq. (6) to obtain $\mathcal{A}(\omega)$, which is to be compared with the respective analytical prediction.

Finite element meshes for the relevant fragments of the composite layers with cylindrical inclusions are depicted in Fig. 6a for the case with impervious inclusions, and in Fig. 6b for the case of porous inclusions (where the mesh of the cylinders is marked in grey). In both cases, the geometry is two-dimensional due to geometric invariance along the axis of the cylindrical inclusions. Moreover, the symmetry is exploited by only modelling the upper halves of the cylinders. Recall

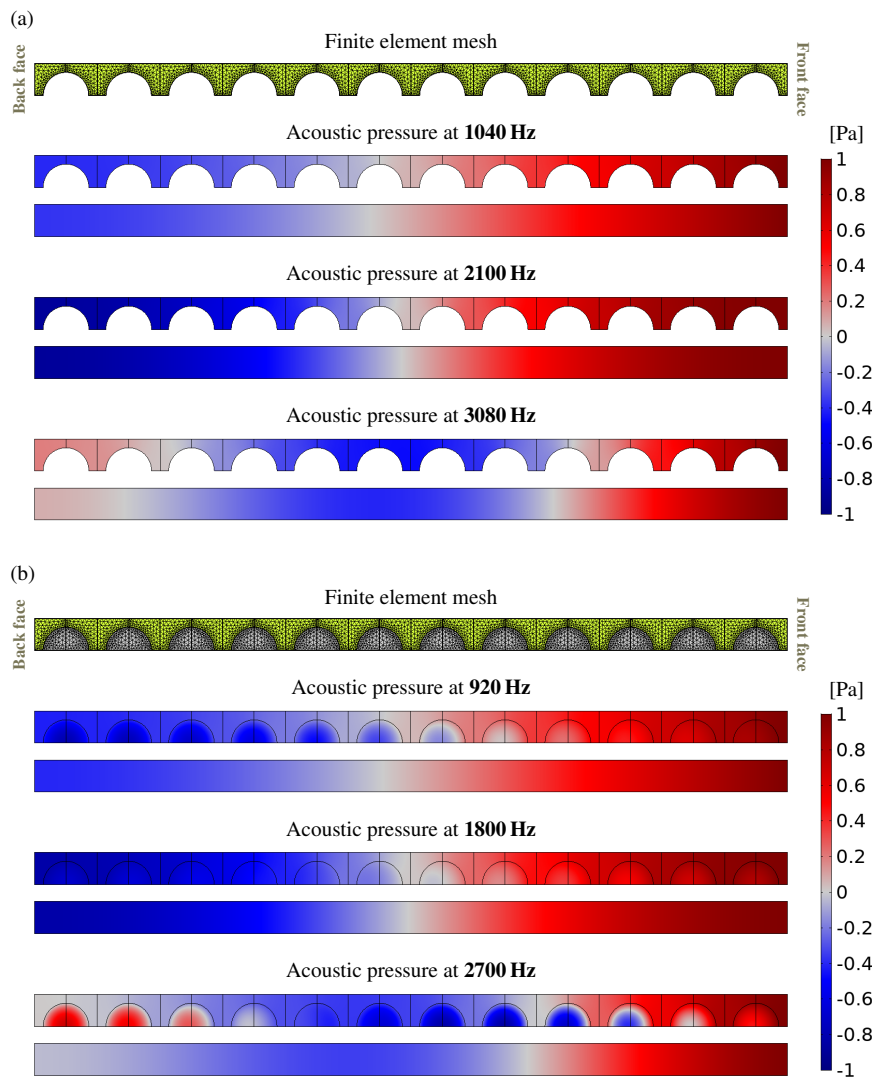


Figure 6: Real part of the acoustic pressure distributions in the porous composite with (a) impervious, or (b) porous cylindrical inclusions, modelled using the shown finite element meshes, and the corresponding pressure fields inside the homogenised layer.

that the cylindrical inclusion radius is $r_i = 2$ mm, while the periodic cell size is $b = 5.5$ mm (leading to $\varphi_m = 0.5846$ and $\varphi_i = 0.4154$). Twelve inclusions (i.e. periodic cells) along the composite layer thickness are considered in this validation example, which means that the layer thickness is $d = 12b = 66$ mm. Fig. 6 also shows the acoustic pressure distributions (at certain frequencies) inside the porous composites with cylindrical inclusions juxtaposed, for comparison, with the corresponding pressure fields inside the homogenised layers equivalent to these composites. The latter has been obtained by solving the Helmholtz equation in a rigidly-backed layer of the porous composite modelled as an equivalent fluid with analytically determined effective wave number.

Similarly, the normalised surface impedances calculated from the finite-element solutions of the porous composite problems for frequencies ranging from 200 Hz up to 3.2 kHz are compared in Fig. 7 with the corresponding analytical predictions, while the curves of the corresponding sound absorption coefficients are compared in Fig. 8. In addition, the normalised surface impedance and absorption curves determined for a porous layer of thickness d , made solely of the fibrous material of the matrix, are shown in the respective graphs to better demonstrate the change in acoustical properties

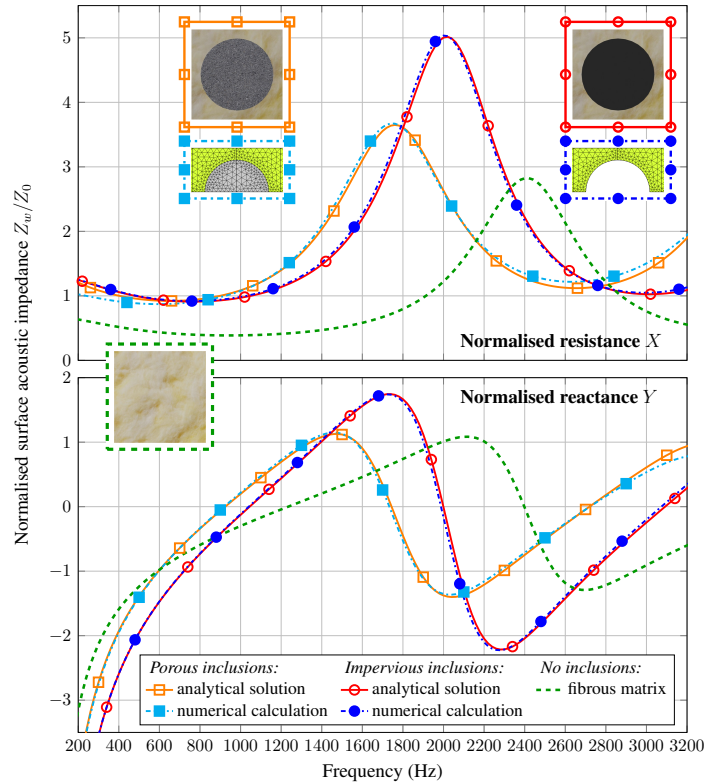


Figure 7: Normalised resistance and reactance of the porous composites with cylindrical inclusions and of the porous matrix material.

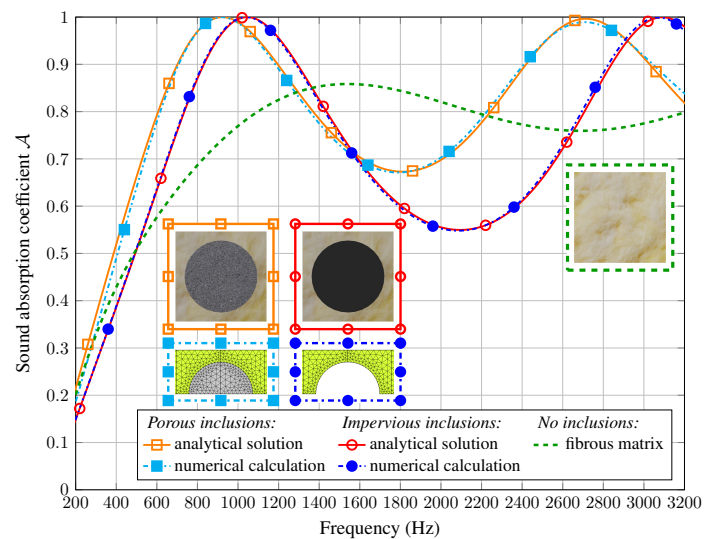


Figure 8: Sound absorption coefficient of rigidly-backed layers of the porous composites with cylindrical inclusions and of the porous matrix material.

due to the introduction of inclusions, which leads to nearly perfect absorption at the peaks, thanks to the rational composite design that permits to achieve the impedance matching condition, as shown in Figs. 7 and 8. The advantage of adding resistive porous inclusions to the highly permeable matrix is clear. In both cases, i.e. the composite with porous cylindrical inclusions as well as the one with impervious inclusions, the corresponding surface impedance and absorption results obtained from the numerical and analytical solutions are nearly identical with only small discrepancies seen mainly at higher frequencies (cf. Figs. 7 and 8). Moreover, a good overall agreement is found between the pressure fields obtained from the direct numerical calculations and the analytical results, compared in Fig. 6. Discrepancies are only visible at the higher frequencies corresponding to the second peak in absorption (i.e. at 3080 Hz in the case of impervious inclusions, or at 2700 Hz for porous inclusions). The discrepancies may be caused by the onset of weak scattering effects [57, 58]. These effects are captured in the direct numerical simulation but are not accounted for in the developed homogenisation-based theory.

Finally, it is worth noting that, contrarily to the case of conventional porous material where the pressure is locally constant, the pressure fields in the porous constituents, shown in Fig. 6b, exhibit significant differences at the first and second absorption peaks frequencies, i.e. at 920 Hz and 2700 Hz. This is a direct consequence of the pressure diffusion phenomenon and is particularly visible at the frequency of the second absorption peak.

Three-dimensional modelling has to be used for numerical validation of the composites with spherical inclusions. Nevertheless, by taking the full advantage of symmetry, the modelled fragment of the composite layer has a small triangular base (i.e. only one eighth of the square base of the cubic periodic cell) and it contains seven inclusions (periodic cells) along the whole layer thickness. The corresponding finite element meshes are shown in Fig. 9a for the impervious inclusion case and in Fig. 9b for the case with porous spherical inclusions (with the mesh of the inclusions marked in grey). Thus, as a consequence of symmetry on all three lateral sides, the modelled geometry contains only representative

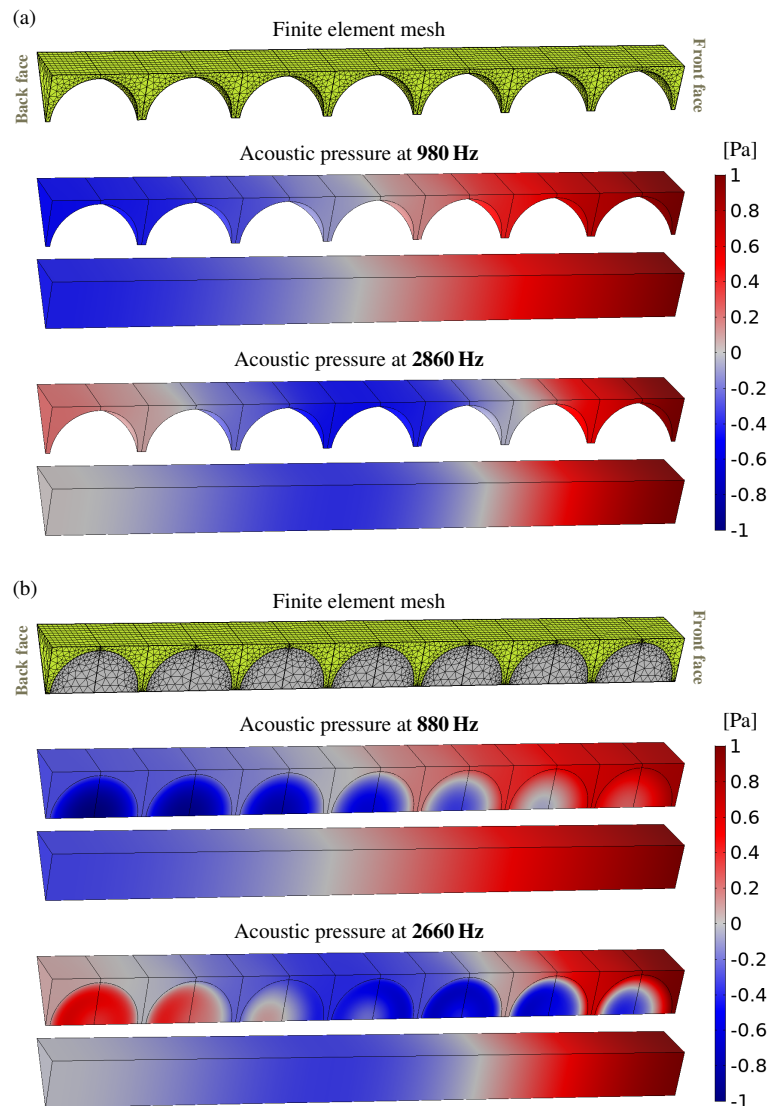


Figure 9: Real part of the acoustic pressure distributions in the porous composite with (a) impervious, or (b) porous spherical inclusions, modelled using the shown finite element meshes, and the corresponding pressure fields inside the homogenised layer.

fragments (sections) of the spherical inclusions. Recall that the spherical inclusion radius is $r_i = 5$ mm, while the periodic cell size is $b = 11$ mm (yielding $\varphi_m = 0.6066$ and $\varphi_i = 0.3934$), and since seven inclusions (periodic cells) along the composite layer thickness are assumed in this validation example, the layer thickness is $d = 7b = 77$ mm. The results of the numerical and analytical solutions of the problem of sound propagation and absorption in such porous composites with spherical inclusions are confronted in the same way as in the previous case of cylindrical inclusions, leading to similar observations, conclusions, and model validation. The normalised surface impedance and sound absorption coefficient are compared in Figs. 10 and 11, respectively, while the sound pressure fields at two frequencies corresponding to the absorption peaks are juxtaposed for comparison in Fig. 9. In particular, note that the sound absorption coefficient of the inclusion material alone is not shown because it takes very small values. The discrepancies between the numerical and analytical results are again very small and mainly at higher frequencies, where a slight shift of \mathcal{A} in frequency is observed at the second absorption peak.

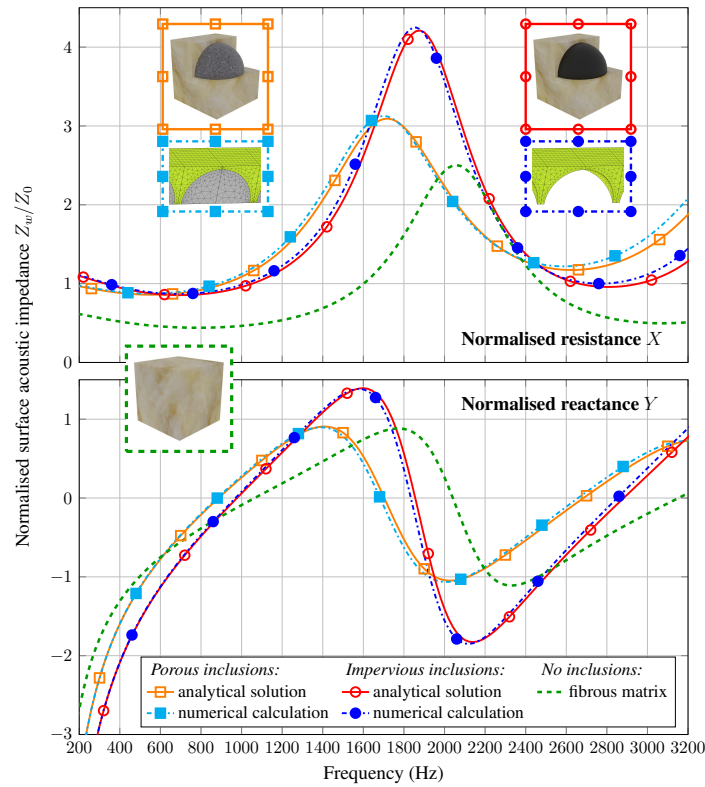


Figure 10: Normalised resistance and reactance of the porous composites with spherical inclusions and of the porous matrix material.

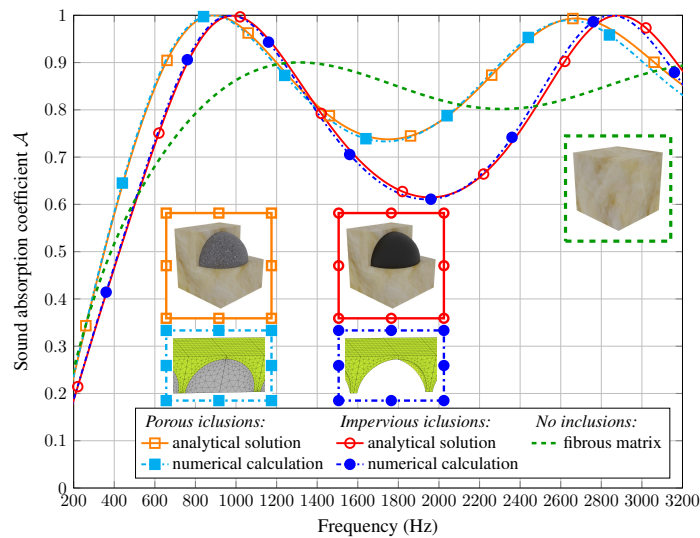


Figure 11: Sound absorption coefficient of rigidly-backed layers of the porous composites with spherical inclusions and of the porous matrix material.

It is emphasised that Fig. 10 exemplifies that adding inclusions to the chosen highly permeable matrix leads to a better match between the real part of the surface impedance of the hard-backed composite layer and the characteristic impedance of air for frequencies around the frequency at which the reactance of the hard-backed composite layer is zero. In turn, this results in a nearly perfect sound absorption coefficient value at the peak frequencies (e.g. at around 880 Hz and 2660 Hz for the composite with weakly permeable inclusions, see Fig. 11), thanks to satisfying the impedance matching condition. It is clear that the acoustic performance of the composite, quantified through the sound absorption coefficient at low frequencies, is improved over that of the chosen highly permeable matrix material alone. Such improved acoustic performance is due to visco-thermal losses in the porous matrix as well as the tortuosity effect induced by the inclusion pattern (i.e. the shape, size and arrangement of inclusions) in composites with impervious inclusions, or due to the visco-thermal losses and both the tortuosity effect and pressure diffusion in composites with weakly permeable inclusions. The tortuosity effect reduces the dynamic viscous permeability of the porous matrix material (or increases its dynamic flow resistivity), leading to a larger value of the real part of the surface impedance at low frequencies. This, together with pressure diffusion in the weakly permeable inclusions, yields a shorter effective wavelength in the composite in comparison with that in the porous matrix material alone. In turn, such a shorter effective wavelength brings as a consequence that the reactance of the hard-backed composite layer takes a zero value at a lower frequency, which results in a sound absorption spectrum with peaks at frequencies lower than those of the absorptive peaks of the hard-backed layer of the porous matrix material alone.

In summary, the results presented in this section not only allow to conclude that the introduced homogenisation-based analytical models capture the physics correctly and can therefore be considered as validated, but also to exemplify the conditions for which rigidly-backed layers of porous composites can be designed to exhibit superior sound absorption performance in comparison with that of layers made from either the porous matrix material or inclusion material alone. If a hard-backed layer of a permeable material has a normalised resistance smaller than 1, then judiciously adding inclusions having a much lower permeability appears as a simple way of both increasing the normalised resistance and decreasing the magnitude of the reactance. This permits both satisfying the impedance matching condition and achieving ideal or nearly-perfect absorption at the peaks with such a designed composite hard-backed layer. One should bear in mind, however, that it is not always possible to improve the acoustic absorption performance of a hard-backed porous matrix by adding weakly permeable inclusions, particularly when its normalised resistance is greater than one.

3.3 Experimental validation

This section experimentally validates the developed theory by comparing the theoretically calculated results with the measured sound absorption coefficient [59] of a rigidly-backed porous composite layer. The experiment was carried out in an impedance tube, according to the procedure described in the standard ISO 10534-2 [60]. Such a commonly used device to measure the normal-incidence sound absorption coefficient of material layers is, in its simplest set up, a closed tube where a loudspeaker generating plane waves is placed on one end of the tube, while the sample is placed on the other end. The acoustic pressure is sensed with a flush-mounted microphone at two positions along the tube. Based on a classical plane-wave decomposition, the transfer function between the two sensed acoustic pressures is related to the reflection coefficient of the hard-backed layer. The reflection coefficient is then used to determine the surface impedance and sound absorption coefficient. For more details about the procedure, the reader is referred to the ISO standard [60].

The sound absorption coefficient measurement reported below was taken in a commercial impedance tube B&K type 4206 (see Fig. 12). The diameter of the impedance tube is 100 mm, which ensured a regime of plane waves under normal incidence in the frequency range [100,2000] Hz. However, the results are reported up to 1300 Hz in order to fully ensure the validity of the long-wavelength assumption the developed theory relies on. The matrix material is a heavy rock wool having a bulk density of 140 kg/m³. A 100-mm-diameter sample was cut with a die cutter to ensure a tight fit in the impedance tube. The inclusion, made from a melamine foam having a bulk density of 10 kg/m³, was cut using a 46-mm diameter die cutter. A careful assembly prevented any air gaps between the matrix and inclusion materials (see Fig 12).

As previously, the dynamic permeabilities of the porous matrix and inclusion materials are calculated with the JCAL model (see Eqs. (C.2) and (C.6) in Appendix C). The input parameters [59] are reported in Table 1. Note that $f_v = \omega_v/2\pi$ and $f_t = \omega_t/2\pi$. Since the static permeability of the porous matrix is comparable to that of the porous inclusion, the effective parameters are calculated from Eqs. (23) and (22). In these calculations: $r_i = 2.3$ cm, $r_m = 5$ cm (see Fig. 12), $\varphi_i = 0.2116$, $\varphi_m = 1 - \varphi_i$, and the layer thickness is $d = 4$ cm.

Material	ϕ [-]	\mathcal{K}_0 [m ²]	f_v [kHz]	M_v [-]	Θ_0 [m ²]	f_t [kHz]	M_t [-]
Matrix	0.97	2.08×10^{-10}	11.22	4.79	1.0×10^{-9}	3.27	3.58
Inclusion	0.98	11.85×10^{-10}	1.98	0.97	2.7×10^{-9}	1.22	0.44

Table 1: Macroparameters of the porous matrix and inclusion materials of the porous composite used for the experimental validation of the developed theory.

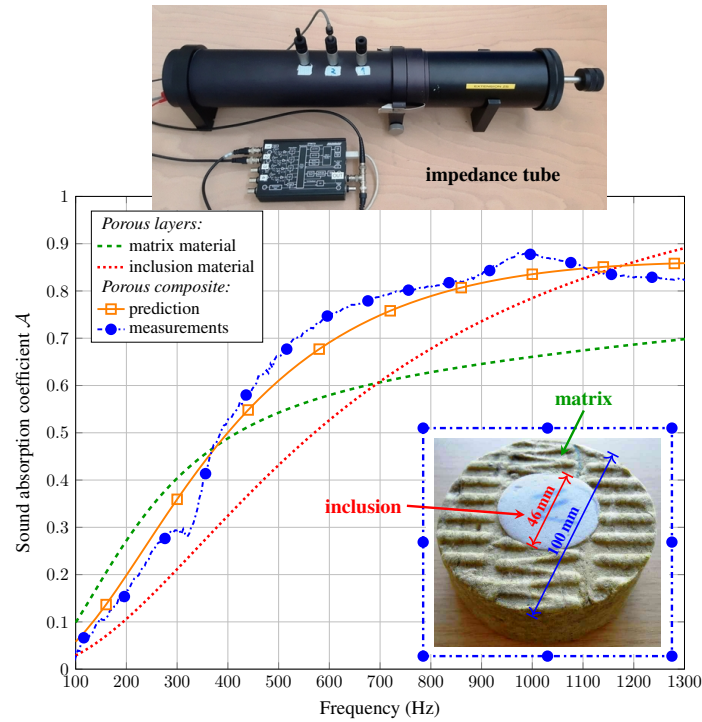


Figure 12: Predicted and measured sound absorption coefficient of a porous composite with cylindrical inclusions. The same acoustical descriptor for the porous matrix and inclusion materials is also plotted for comparison. The measured sample and the impedance tube are shown as inset images.

Figure 12 compares the analytically predicted and measured values of the sound absorption coefficient of the porous composite. Direct finite-element results have also been successfully compared to the analytical predictions but, for the sake of clarity, the purely numerical results are not shown in the plot.

It is clear that the analytical prediction closely agrees with the measured data. The relative error is smaller than 5% in frequencies higher than 400 Hz. For lower frequencies, the results tend to differ more, specially around 300 Hz. This is explained by the fact that the analytical model assumes that the solid frame of the porous constituents is perfectly rigid and motionless, while the local minimum that appears in the measured data around 300 Hz is caused by the vibration of the elastic frame of the porous constituents, i.e. due to poroelastic effects. It is also relevant that the analytical prediction and measured sound absorption coefficient of the composite are shown to be higher than that of both the porous matrix and inclusion materials, particularly in middle-range frequencies around 600 Hz. This is a direct consequence of the visco-thermal dissipation occurring in each porous constituent. In summary, the theory can be considered as experimentally validated.

4 Conclusions

In this work, the macroscopic equations that govern acoustic wave propagation in rigid-frame porous composites with arbitrary but periodic geometry were derived by using the two-scale asymptotic homogenisation method. Analytical models for the acoustical properties of porous composites comprising a matrix with periodically embedded cylindrical or spherical inclusions were introduced. The predictions of these models closely agreed with both the results of direct finite-element simulations and experimental testing. In addition, the conditions for which rigidly-backed layers of porous composites can present superior sound absorption performance in comparison with that of layers made from their individual constituents were determined. Based on the theoretical analysis and the numerical and experimental verifications, the following main conclusions are drawn:

1. In composites with constituents characterised by highly contrasted permeabilities, the presence of the inclusions leads to i) a decrease of the dynamic viscous permeability of the highly permeable matrix due to both the tortuosity effect and the reduction of the volume fraction of the matrix, and ii) the emergence of pressure diffusion which alters the effective compressibility of the composite.
2. In composites with constituents that have weakly contrasted permeabilities and particular geometries, their dynamic permeability can be, depending on the permeability of the inclusions and the space these take up, either decreased or increased with respect to the permeability of the porous matrix material, while their effective compressibility is determined by a simple mixture law.

3. The developed theory both rigorously captures the acoustic interaction between the porous constituents of the composite, and permits to elucidate the physical mechanisms underlying the dissipation of sound energy in rigid-frame porous composites. These correspond to classical visco-thermal dissipation in the constituents together with, for composites characterised by highly contrasted permeabilities, pressure diffusion which provides additional and tunable sound energy dissipation.

In summary, this work provides a theoretical framework to guide the rational design of optimised noise mitigation solutions for engineering applications where the space is limited. One should note, however, that the developed theory neither describes the acoustical properties of porous composites with different types of porous inclusions per representative elementary volume (which could represent highly heterogeneous porous composites) nor considers the elasticity of the solid frame of the porous constituents. Research on these topics may be undertaken to extend the results of this work.

Acknowledgements

This work has been financially supported by the National Agency for Research and Development (ANID) through FONDECYT Grant No. 1211310. R. Venegas and G. Núñez also acknowledge the financial support from Corporación de Fomento de la Producción CORFO Chile (Production Development Corporation) through grant 16ENI2-66903 Innov-Ing2030. T. G. Zieliński acknowledges the financial support from the project “Relations between the micro-geometry and sound propagation and absorption in porous and poroelastic media”, under Grant Agreement No. 2015/19/B/ST8/03979 by the National Science Centre (NCN), Poland. The COST action CA15125 (DENORMS) initiated and facilitated this work.

A Upscaling of the wave equation in porous composites with highly contrasted permeabilities

A.1 Physical analysis

The purpose of the physical analysis of the local description, i.e. Eqs. (8)–(13), is to determine whether the variables fluctuate locally or macroscopically as well as the relative order of magnitude of the different terms in the equations. This analysis will be used in the rescaling of the local description to be upscaled.

Assuming that the porous matrix is much more permeable than the porous inclusions, i.e. $|\mathbf{k}_m| \gg |\mathbf{k}_i|$, implies that the porous matrix carries the long wave while the pressure in the porous inclusions varies locally. As a consequence, the pressure in the porous matrix fluctuates at the macroscopic scale with the sound wavelength and this leads to the following estimate $|\nabla p_m| = O(p_m/L)$. On the other hand, while the Darcy velocity in the porous matrix, estimated as $V_m = |\mathbf{V}_m|$, fluctuates at the local scale, its divergence varies with the sound wavelength and, consequently, it can be estimated as $|\nabla \cdot \mathbf{V}_m| = O(V_m/L)$. Moreover, the terms in the mass balance Eq. (8) are of the same order of magnitude, i.e. $O(V_m/L) = O(|\omega p_m C_m|)$, which is also the case for those in the Darcy’s law (9), i.e. $O(V_m) = O(|\mathbf{k}_m p_m / \eta L|)$.

In the porous inclusion, the Darcy velocity \mathbf{V}_i and the pressure p_i fluctuate at the local scale. Moreover, the terms in the mass balance equation (10), as well as those in the dynamic Darcy’s law (11), are of the same order of magnitude, i.e. $O(V_i/\ell) = O(|\omega p_i C_i|)$ and $O(V_i) = O(|\mathbf{k}_i p_i / \eta \ell|)$, respectively. Combining these estimates reveal that the porous inclusions experience local dynamics around the characteristic frequency $\omega = O(|\mathbf{k}_i / \eta C_i \ell^2|)$.

On the interface Γ , the continuity of pressure results in $O(p_p) = O(p_i)$ while the long-wavelength condition imposes that the Darcy velocity in the porous inclusions is, in terms of the small parameter ε , of one order lower than the Darcy velocity generated by the incident wave in the porous matrix, i.e. $\mathcal{V} = |\mathbf{V}_i \cdot \mathbf{n}| / |\mathbf{V}_m \cdot \mathbf{n}| = O(\varepsilon)$. In terms of physical parameters, the ratio \mathcal{V} can be written as $\mathcal{V} = |\mathbf{k}_i p_i / \eta \ell| / |\mathbf{k}_m p_m / \eta L| = \varepsilon^{-1} |\mathbf{k}_i| / |\mathbf{k}_m| = O(\varepsilon)$, which is consistent with the physical estimation of \mathcal{V} provided that the ratio between the permeabilities of the porous inclusion and matrix is of the order of ε^2 , i.e. the permeabilities are highly contrasted. As in double porosity [34–37] or multiporosity media [38–40], permeability ratio values in the order of 10^{-6} – 10^{-4} suffice to satisfy the estimation of \mathcal{V} .

A.2 Rescaled local description

Following the presentation of the homogenisation procedure applied to multiscale porous media in [39, 40], one observes that the scale separation between the local and macroscopic characteristic sizes, i.e. $\ell/L = \varepsilon \ll 1$, permits the use of the two-scale asymptotic method of homogenisation to derive an equivalent macroscopic model [11] starting from the set of equations presented in §2.2 that governs the physics of acoustic wave propagation in the porous composite.

To account for the evolution at the two spatial scales, one can take the macroscopic characteristic length L as the reference length and use the dimensional space variables x (i.e. the usual space variable) and $y = \varepsilon^{-1}x$ to describe the variations at the (slow) macroscopic and (fast) local scales, respectively. Then, the usual vector differential operator is changed into $\nabla = \nabla_x + \varepsilon^{-1}\nabla_y$. On the other hand, the use of the two space variables is combined with a rescaling of the

local equations based upon only one of them and the physical analysis. The rescaling is justified because when expressed with the two space variables (x, y) , the actual physical gradient of a quantity Q that varies macroscopically, i.e. $\nabla_x Q$, becomes ∇Q . On the other hand, if the quantity varies at the local scale, the actual physical gradient $\nabla_y Q$ should be expressed as $\varepsilon \nabla Q$. Therefore, the gradient of variables oscillating at the local scale is rescaled.

Adopting the usual homogenisation convention of keeping the same notation as for the single-space-variable formulation for both the variables and the gradient operator, the rescaled local description of wave propagation in the porous composite, comprising the rescaled equations of conservation of mass (A.1) and (A.3), Darcy's laws (A.2) and (A.4), and boundary conditions (A.5) and (A.6), is given by (with $\nabla = \nabla_x + \varepsilon^{-1} \nabla_y$)

$$\nabla \cdot \mathbf{V}_m + j\omega p_m C_m(\omega) = 0 \quad \text{in } \Omega_m, \quad (\text{A.1})$$

$$\mathbf{V}_m = -\frac{\mathbf{k}_m(\omega)}{\eta} \cdot \nabla p_m \quad \text{in } \Omega_m, \quad (\text{A.2})$$

$$\varepsilon \nabla \cdot \mathbf{V}_i + j\omega p_i C_i(\omega) = 0 \quad \text{in } \Omega_i, \quad (\text{A.3})$$

$$\mathbf{V}_i = -\frac{\mathbf{k}_i(\omega)}{\eta} \cdot \varepsilon \nabla p_i \quad \text{in } \Omega_i, \quad (\text{A.4})$$

$$\mathbf{V}_m \cdot \mathbf{n} = \varepsilon \mathbf{V}_i \cdot \mathbf{n} \quad \text{on } \Gamma, \quad (\text{A.5})$$

$$p_m = p_i \quad \text{on } \Gamma. \quad (\text{A.6})$$

In particular, it should be noted here that the divergence of the Darcy velocity in Eq. (A.1) is not rescaled since, as previously discussed, it varies with the sound wavelength. On the other hand, the ε -scaling in Eqs. (A.3) and (A.4) is due to the fact that the respective Darcy velocity and pressure vary locally and consequently the gradient operator is rescaled, while the ε -scaling in Eq. (A.5) accounts for the physical estimate of \mathcal{V} , as discussed in the previous section.

A.3 Boundary-value problems

The unknown variables are looked for in the form of series expansion in terms of the small parameter ε , i.e. as $Q = \sum_k \varepsilon^k Q^{(k)}$, where $k = 0, 1, \dots$, and the superscript (k) indicates the order of approximation, while $Q = \{\mathbf{V}_m, p_m, \mathbf{V}_i, p_i\}$. The unknown variables are then inserted into Eqs. (A.1)–(A.6) and the terms of the same order are identified.

At ε^{-1} , it follows from Eq. (A.2) that $\nabla_y p_m^{(0)} = \mathbf{0}$. Hence, the pressure in the porous matrix is a macroscopic variable, i.e. $p_m^{(0)} = p_m^{(0)}(x)$. Further identification leads to the following problem

$$\nabla_y \cdot \mathbf{V}_m^{(0)} = 0 \quad \text{in } \Omega_m, \quad (\text{A.7})$$

$$\mathbf{V}_m^{(0)} = -\frac{\mathbf{k}_m(\omega)}{\eta} \cdot (\nabla_x p_m^{(0)} + \nabla_y p_m^{(1)}) \quad \text{in } \Omega_m, \quad (\text{A.8})$$

$$\mathbf{V}_m^{(0)} \cdot \mathbf{n} = 0 \quad \text{on } \Gamma, \quad (\text{A.9})$$

which can be rewritten as

$$\nabla_y \cdot (\nabla_y p_m^{(1)} + \nabla_x p_m^{(0)}) = 0 \quad \text{in } \Omega_m, \quad (\text{A.10})$$

$$(\nabla_y p_m^{(1)} + \nabla_x p_m^{(0)}) \cdot \mathbf{n} = 0 \quad \text{on } \Gamma. \quad (\text{A.11})$$

To determine the equivalent weak formulation of this problem, Eq. (A.10) is multiplied by a test Ω -periodic pressure field q , the resulting equation is integrated over Ω_m , and the divergence theorem is used to obtain

$$\int_{\partial\Omega_m} q(\nabla_y p_m^{(1)} + \nabla_x p_m^{(0)}) \cdot \mathbf{n} d\Gamma - \int_{\Omega_m} (\nabla_y p_m^{(1)} + \nabla_x p_m^{(0)}) \cdot \nabla_y q d\Omega = 0. \quad (\text{A.12})$$

The first integral vanishes because of the periodicity and the boundary condition (A.11). Hence, one has that

$$\int_{\Omega_m} \nabla_y p_m^{(1)} \cdot \nabla_y q d\Omega = - \int_{\Omega_m} \nabla_x p_m^{(0)} \cdot \nabla_y q d\Omega. \quad (\text{A.13})$$

The Lax-Milgram theorem ensures the existence and uniqueness of the solution of this problem of conduction through a matrix with non-conducting inclusions [30]. The solution is given by

$$p_m^{(1)} = \boldsymbol{\xi}(y) \cdot \nabla_x p_m^{(0)}, \quad (\text{A.14})$$

where the three components of the zero-mean vector $\boldsymbol{\xi}$ are the solutions for unitary pressure gradient in the three spatial directions. Note that a constant in the solution Eq. (A.14) has been omitted since it has no influence on further calculations.

Inserting Eq. (A.14) into Eq. (A.8) yields the leading-order Darcy velocity in the porous matrix, i.e.

$$\mathbf{V}_m^{(0)} = -\frac{\mathbf{k}_m}{\eta} \cdot (\nabla_y \boldsymbol{\xi}(y) + \mathbf{I}) \cdot \nabla_x p_m^{(0)}, \quad (\text{A.15})$$

where \mathbf{I} is the second-rank unitary tensor.

From Eqs. (A.3), (A.4) and (A.6), one identifies the following boundary-value problem for the pressure in the porous inclusion

$$\nabla_y \cdot (\mathbf{D} \cdot \nabla_y p_i^{(0)}) = j\omega p_i^{(0)} \quad \text{in } \Omega_i, \quad (\text{A.16})$$

$$p_i^{(0)} = p_m^{(0)} \quad \text{on } \Gamma. \quad (\text{A.17})$$

where $\mathbf{D} = \mathbf{k}_i/\eta\mathcal{C}_i$ is the pressure diffusivity tensor, which for isotropic porous inclusions reduces to $\mathbf{D} = \mathcal{D}\mathbf{I}$ with $\mathcal{D} = \mathcal{K}_i/\eta\mathcal{C}_i$ and $\mathbf{k}_i = \mathcal{K}_i\mathbf{I}$. Considering the latter approximation (for simplicity) and the auxiliary variable $P = p_i^{(0)} - p_m^{(0)}$, the pressure diffusion problem is rewritten as

$$\nabla_y \cdot (\mathcal{D}\nabla_y P) - j\omega P = j\omega p_m^{(0)} \quad \text{in } \Omega_i, \quad (\text{A.18})$$

$$P = 0 \quad \text{on } \Gamma. \quad (\text{A.19})$$

This a linear problem forced by the porous matrix macroscopic pressure $p_m^{(0)}$. Hence, as in [33, 34, 39, 40], the unknown P can be linearly related to $p_m^{(0)}$ via

$$P = -\frac{\bar{b}(y, \omega)}{\mathcal{D}} j\omega p_m^{(0)}, \quad (\text{A.20})$$

where \bar{b} carries units of m^2 and represents the unknown Ω -periodic local diffusive pressure field [34, 39, 40] normalised by $-j\omega p_m^{(0)}/\mathcal{D}$. Using the original variables, Eq. (A.20) can be rewritten as

$$p_i^{(0)} = p_m^{(0)} \left(1 - \frac{j\omega \bar{b}(y, \omega)}{\mathcal{D}} \right). \quad (\text{A.21})$$

A.4 Derivation of the macroscopic effective equations

Applying the following averaging operator

$$\langle \cdot \rangle = \frac{1}{\Omega} \int_{\Omega_m} \cdot d\Omega, \quad (\text{A.22})$$

to the mass balance equation (A.1) identified at ε^0 leads to

$$\nabla_x \cdot \langle \mathbf{V}_m^{(0)} \rangle + \langle \nabla_y \cdot \mathbf{V}_m^{(1)} \rangle + j\omega p_m^{(0)} \varphi_m \mathcal{C}_m = 0. \quad (\text{A.23})$$

The term $\langle \nabla_y \cdot \mathbf{V}_m^{(1)} \rangle$ in Eq. (A.23) is calculated by making successive use of the divergence theorem, noting that the surface integrals on the opposite boundaries of the cell cancel out due to periodicity, and using Eq. (A.5) at ε^1 , i.e. $\mathbf{V}_m^{(1)} \cdot \mathbf{n} = \mathbf{V}_i^{(0)} \cdot \mathbf{n}$ on Γ , and Eq. (A.3) at ε^0 . The final result is

$$\langle \nabla_y \cdot \mathbf{V}_m^{(1)} \rangle = j\omega \mathcal{C}_i \frac{1}{\Omega} \int_{\Omega_i} p_i^{(0)} d\Omega. \quad (\text{A.24})$$

Combining Eqs. (A.21), (A.24) and (A.23) one obtains the macroscopic mass balance equation (14).

On the other hand, applying the operator (A.22) to Eq. (A.15) at ε^0 leads to the dynamic Darcy's law (18), for which the dynamic viscous permeability tensor is calculated as

$$\mathbf{k} = \langle \mathbf{k}_m \cdot (\nabla_y \boldsymbol{\xi}(y) + \mathbf{I}) \rangle = \varphi_m \mathbf{k}_m \cdot \boldsymbol{\Psi}, \quad (\text{A.25})$$

where the tensor $\boldsymbol{\Psi}$ is defined as

$$\boldsymbol{\Psi} = \frac{1}{\Omega_m} \int_{\Omega_m} (\nabla_y \boldsymbol{\xi}(y) + \mathbf{I}) d\Omega. \quad (\text{A.26})$$

Noting that the leading-order boundary value problem (A.10)–(A.11) is formally identical to a potential flow problem (see §9.4.4.3 in [11], and in particular Eq. 9.15 and the related discussion), the tensor $\boldsymbol{\Psi}$ is directly identified as the inverse of the tortuosity tensor α_∞ induced by the presence of the inclusions. Hence, the dynamic viscous permeability tensor can be rewritten as in Eq. (19). Note that this result was also found in [31] but for the case of an array of Helmholtz resonators.

As a remark, the derivation of the macroscopic description of wave propagation in porous composites comprising a porous matrix and a single perfectly impervious inclusion per REV is outlined. For such a case, the local description is given by Eqs. (8)–(9), together with Eq. (12) being replaced by $\mathbf{V}_m \cdot \mathbf{n} = 0$ on Γ . The rescaled local description is given by Eqs. (A.1)–(A.2) and $\mathbf{V}_m \cdot \mathbf{n} = 0$ on Γ . The homogenisation procedure closely follows that described in the previous sections, with the particularity that $\langle \nabla_y \cdot \mathbf{V}_m^{(1)} \rangle$ in Eq. (A.23) is null. Finally, the macroscopic description is given by Eqs. (14) and (18), where the effective compressibility and dynamic viscous permeability are given by Eqs. (20) and (19), respectively.

B Upscaling of the wave equation in porous composites with weakly contrasted permeabilities

The upscaling of acoustic wave propagation in porous composites with weakly contrasted permeabilities, i.e. $|\mathbf{k}_i| = O(|\mathbf{k}_m|)$, and $|C_i| = O(|C_m|)$ is succinctly presented in this section. The local description is as in §2.2 while the physical analysis closely follows that presented in §A.1, with the difference being that the incident wave is carried by both the porous matrix and inclusions. This means that the pressure (in both constituents) varies with the sound wavelength which is also the case of the divergence of the velocities and this allows to account for the macroscopic compressibility of the composite. Furthermore, the continuity of velocity and pressure on Γ leads, in this case, to the estimate $\mathcal{V} = O(1)$ and the rescaled local description given by Eqs. (8)–(13) (with $\nabla = \nabla_x + \varepsilon^{-1}\nabla_y$). Having inserted the series into the rescaled description, the identification process yields at ε^{-1} that $\nabla_y p_m^{(0)} = \mathbf{0}$ and $\nabla_y p_i^{(0)} = \mathbf{0}$. Hence, the pressure in the constituents is a macroscopic variable, i.e. $p_m^{(0)} = p_m^{(0)}(x) = p^{(0)}$ and $p_i^{(0)} = p_i^{(0)}(x) = p^{(0)}$. Further identification leads to the following coupled problem (with $u = m, i$)

$$\nabla_y \cdot \mathbf{V}_u^{(0)} = 0 \quad \text{in } \Omega_u \quad \text{with} \quad \mathbf{V}_u^{(0)} = -\eta^{-1} \mathbf{k}_u \cdot (\nabla_y p_u^{(1)} + \nabla_x p^{(0)}), \quad (\text{B.1})$$

$$\mathbf{V}_m^{(0)} \cdot \mathbf{n} = \mathbf{V}_i^{(0)} \cdot \mathbf{n} \quad \text{and} \quad p_m^{(1)} = p_i^{(1)} \quad \text{on } \Gamma. \quad (\text{B.2})$$

This a conduction problem [11] that is linear and forced by the macroscopic pressure gradient [see the equation 4.25 in [11] for its weak formulation]. The solution can then be written as Eq. (A.14). It then follows that the leading-order velocities are given by $\mathbf{V}_u^{(0)} = -\eta^{-1} \mathbf{k}_u \cdot (\nabla_y \xi_u(y) + \mathbf{I}) \cdot \nabla_x p^{(0)}$. Spatially averaging the overall velocity $\mathbf{V}^{(0)}$ ($= \mathbf{V}_u^{(0)}$ in Ω_u , with $u = m, i$), one obtains the macroscopic Darcy's law (18) (with $\mathbf{V}_m^{(0)}$ replaced by $\mathbf{V}^{(0)}$) for which the dynamic viscous permeability tensor is calculated as in Eq. (23), i.e. $\mathbf{k} = \varphi_m \mathbf{k}_m \cdot \Xi_m + \varphi_i \mathbf{k}_i \cdot \Xi_i$. Here the tensors Ξ_u (with $u = m, i$) are defined as

$$\Xi_u = \frac{1}{\Omega_u} \int_{\Omega_u} (\nabla_y \xi(y) + \mathbf{I}) d\Omega. \quad (\text{B.3})$$

In general, these tensors are complex valued and depend on frequency and the geometry of the matrix and inclusions. However, for composites with inclusions having constant cross-section and sound propagation in the direction along the inclusions axis, one has that $\Xi_m = \Xi_m \mathbf{I}$ and $\Xi_i = \Xi_i \mathbf{I}$, which means that for such composites the dynamic viscous permeability is given by a simple mixture law.

C Effective parameters of the porous composites constituents

For the sake of brevity, the dynamic permeabilities of the porous constituents are calculated using semi-phenomenological models [7, 10] based on the scaling function \mathcal{X} given by

$$\mathcal{X}(\omega, \mathcal{X}_0, \varpi, \mathcal{M}) = \mathcal{X}_0 \left(\frac{j\omega}{\varpi} + \sqrt{1 + \frac{j\omega}{\varpi} \frac{\mathcal{M}}{2}} \right)^{-1}, \quad (\text{C.1})$$

where $\mathcal{X}_0 = \mathcal{X}(\omega = 0)$, ϖ is a characteristic frequency, and \mathcal{M} is a shape factor.

The porous matrix is assumed as made of a fibrous material with regularly arranged cylindrical fibres [54]. Its porosity is ϕ_m and the fiber radius is a_m . Sound propagation perpendicular to the fibres axis is considered. The dynamic viscous and thermal permeabilities are calculated as

$$\mathcal{K}_m(\omega) = \mathcal{X}(\omega, \mathcal{K}_{0m}, \omega_{vm}, M_{vm}), \quad \Theta_m(\omega) = \mathcal{X}(\omega, \Theta_{0m}, \omega_{tm}, M_{tm}), \quad (\text{C.2})$$

where the input parameters are given by [54]

$$\mathcal{K}_{0m} = a_m^2 \frac{(-2 \ln(1 - \phi_m) - 2\phi_m - \phi_m^2)}{16(1 - \phi_m)}, \quad \Theta_{0m} = 2\mathcal{K}_{0m}, \quad (\text{C.3})$$

$$\omega_{vm} = \frac{\nu}{\mathcal{K}_{0m}} \frac{\phi_m}{2 - \phi_m}, \quad \omega_{tm} = \frac{2 - \phi_m}{2} \frac{\omega_{vm}}{\text{Pr}}, \quad (\text{C.4})$$

$$M_{vm} = 32 \frac{\mathcal{K}_{0m}}{a_m^2} \frac{(1 - \phi_m)^2}{\phi_m^3 (2 - \phi_m)}, \quad M_{tm} = M_{vm} \frac{2 - \phi_m}{2}. \quad (\text{C.5})$$

Here, ν and Pr are the kinematic viscosity and Prandtl number of the saturating gas, respectively. Note that Eq. (21) is used in conjunction with Eqs. (C.2)–(C.5) to calculate C_m .

The porous inclusions are assumed as made of a granular material with porosity ϕ_i and grain radius a_i . The dynamic viscous and thermal permeabilities are calculated as

$$\mathcal{K}_i(\omega) = \mathcal{X}(\omega, \mathcal{K}_{0i}, \omega_{vi}, M_{vi}), \quad \Theta_i(\omega) = \mathcal{X}(\omega, \Theta_{0i}, \omega_{ti}, M_{ti}), \quad (\text{C.6})$$

where the input parameters are given by

$$\mathcal{K}_{0i} = \frac{a_i^2}{3\beta_i^2} \left(\frac{2 + 3\beta_i^5}{\beta_i(3 + 2\beta_i^5)} - 1 \right), \quad \Theta_{0i} = \frac{a_i^2}{15} \frac{(5 - 9\beta_i + 5\beta_i^3 - \beta_i^6)}{\beta_i^3}, \quad (\text{C.7})$$

$$\omega_{vi} = 2 \frac{\nu}{\mathcal{K}_{0i}} \frac{1 - \beta_i^3}{2 + \beta_i^3}, \quad \omega_{ti} = (1 - \beta_i^3) \frac{\alpha}{\Theta_{0i}}, \quad (\text{C.8})$$

$$M_{vi} = 81 \frac{\mathcal{K}_{0i}}{a_i^2} \frac{\beta_i^6}{(2 + \beta_i^3)(1 - \beta_i^3)^3}, \quad M_{ti} = 18 \frac{\Theta_{0i}}{a_i^2} \frac{\beta_i^6}{(1 - \beta_i^3)^3}, \quad (\text{C.9})$$

with $\beta_i = (1 - \phi_i)^{1/3}$. Note that C_i is calculated using Eqs. (21) and (C.6)–(C.9). However, it should be noticed that if $\omega \ll \omega_{vi}$, one can approximate the dynamic viscous permeability and compressibility by their static values \mathcal{K}_{0i} and ϕ_i/P_0 , respectively. Then, consequently, the pressure diffusivity is approximated as $\mathcal{D} = \mathcal{D}_0 = \mathcal{K}_{0i}P_0/\eta\phi_i$.

References

- [1] Allard, J. F.; Atalla, N. Propagation of Sound in Porous Media. Modeling Sound Absorbing Materials, 2nd ed. John Wiley & Sons, 2009.
- [2] Tang, X.; Yan, X. Acoustic energy absorption properties of fibrous materials; A review. *Compos Part A Appl Sci Manuf* 2017; 101:360–380.
- [3] Cox, T. J.; D'Antonio, P. Acoustic Absorbers and Diffusers; Theory, Design and Application, 3rd ed. CRC Press, 2016.
- [4] Biot, M. A. Theory of propagation of elastic waves in a fluid-saturated porous solid. I. Low-frequency range. *J Acoust Soc Am* 1956; 28:168–178.
- [5] Biot, M. A. Theory of propagation of elastic waves in a fluid-saturated porous solid. II. Higher frequency range. *J Acoust Soc Am* 1956; 28:179–191.
- [6] Auriault, J. L.; Borne, L.; Chambon, R. Dynamics of porous saturated media, checking of the generalized law of Darcy. *J Acoust Soc Am* 1985; 77:1641–1650.
- [7] Johnson, D. L.; Koplik, J.; Dashen, R. Theory of dynamic permeability and tortuosity in fluid-saturated porous media. *J Fluid Mech* 1987; 176:379–402.
- [8] Champoux, Y.; Allard, J. F. Dynamic tortuosity and bulk modulus in air-saturated porous media. *J Appl Phys* 1991; 70:1975–1979.
- [9] Pride, S. R.; Morgan, F. D.; Gangi, A. F. Drag forces of porous-medium acoustics. *Phys Rev B* 1993; 47:4964–4975.
- [10] Lafarge, D.; Lemariniere, P.; Allard, J. F.; Tarnow, V. Dynamic compressibility of air in porous structures at audible frequencies. *J Acoust Soc Am* 1997; 102:1995–2006.
- [11] Auriault, J. L.; Boutin, C.; Geindreau, C. Homogenization of Coupled Phenomena in Heterogeneous Media. ISTE Ltd and John Wiley & Sons, 2009.
- [12] Sanchez-Palencia, E. Non-Homogeneous Media and Vibration Theory. Springer-Verlag, 1980.
- [13] Perrot, C.; Panneton, R.; Olny, X. Periodic unit cell reconstruction of porous media; Application to open-cell aluminum foams. *J Appl Phys* 2007; 101:113538.
- [14] Perrot, C.; Chevillotte, F.; Panneton, R. Dynamic viscous permeability of an open-cell aluminum foam. Computations versus experiments. *J Appl Phys* 2008; 103:024909.
- [15] Perrot, C.; Chevillotte, F.; Panneton, R. Bottom-up approach for microstructure optimization of sound absorbing materials. *J Acoust Soc Am* 2008; 124:940–948.
- [16] Venegas, R. Microstructure influence on acoustical properties of multiscale porous materials. Ph.D. thesis, University of Salford, Salford, United Kingdom, 2011.
- [17] Zieliński, T. G.; Venegas, R.; Perrot, C.; Cervenka, M.; Chevillotte, F.; Attenborough, K. Benchmarks for microstructure-based modelling of sound absorbing rigid-frame porous media. *J Sound Vib* 2020; 483:115441.
- [18] Ren, S.; Ao, Q.; Meng, H.; Xin, F.; Huang, L.; Zhang, C.; Lu, T. J. A semi-analytical model for sound propagation in sintered fiber metals. *Compos B Eng* 2017; 126:17–26.
- [19] Sun, X.; Liang, W. Cellular structure control and sound absorption of polyolefin microlayer sheets. *Compos B Eng* 2016; 87:21–26.
- [20] Tang, X.; Yan, X. Multi-layer fibrous structures for noise reduction. *J Text I* 2017; 108:2096–2106.
- [21] Elliott, A. S.; Venegas, R.; Groby, J. P.; Umnova, O. Omnidirectional acoustic absorber with a porous core and a graded index matching layer. *J Appl Phys* 2014; 115:204902.
- [22] Liu, Z.; Zhang, X.; Mao, Y.; Zhu, Y. Y.; Yang, Z.; Chan, C. T.; Sheng, P. Locally resonant sonic materials. *Science* 2000; 289:1734–1736.
- [23] Fang, N.; Xi, D.; Xu, J.; Ambati, M.; Srituravanich, W.; Sun, C.; Zhang, X. Ultrasonic metamaterials with negative modulus. *Nat Mater* 2006; 5:452–456.
- [24] Ma, G.; Sheng, P. Acoustic metamaterials ; From local resonances to broad horizons. *Sci Adv* 2016; 2:e1501595.
- [25] Cummer, S. A.; Christensen, J.; Alù, A. Controlling sound with acoustic metamaterials. *Nat Rev Mater* 2016; 1:16001.
- [26] Ding, Y.; Statharas, E. C.; Yao, K.; Hong, M. A broadband acoustic metamaterial with impedance matching layer of gradient index. *Appl Phys Lett* 2017; 110: 241903.

- [27] Dupont, T.; Leclaire, P.; Sicot, O.; Gong, X. L.; Panneton, R. Acoustic properties of air-saturated porous materials containing dead-end porosity. *J Appl Phys* 2011; 110:094903.
- [28] Groby, J. P.; Lardeau, A.; Huang, W.; Auregan, Y. The use of slow sound to design simple sound absorbing materials. *J Appl Phys* 2015; 117:124903.
- [29] Li, Y.; Assouar, B. M. Acoustic metasurface-based perfect absorber with deep subwavelength thickness. *Appl Phys Lett* 2016; 108:063502.
- [30] Boutin, C. Acoustics of porous media with inner resonators. *J Acoust Soc Am* 2013; 134:4717–4729.
- [31] Boutin, C.; Bécot, F. X. Theory and experiments on poro-acoustics with inner resonators. *Wave Motion* 2015; 54:76–99.
- [32] Venegas, R.; Boutin, C. Acoustics of permeo-elastic materials. *J Fluid Mech* 2017; 828:135–174.
- [33] Boutin, C.; Royer, P.; Auriault, J. L. Acoustic absorption of porous surfacing with dual porosity. *Int J Solids Struct* 1998; 35:4709–4737.
- [34] Olly, X.; Boutin, C. Acoustic wave propagation in double porosity media. *J Acoust Soc Am* 2003; 113:73–89.
- [35] Venegas, R.; Umnova, O. Acoustical properties of double porosity granular materials. *J Acoust Soc Am* 2011; 130:2765–2776.
- [36] Venegas, R.; Umnova, O. Influence of sorption on sound propagation in granular activated carbon. *J Acoust Soc Am* 2016; 140:755–766.
- [37] Venegas, R.; Boutin, C. Acoustics of sorptive porous materials. *Wave Motion* 2017; 68:162–181.
- [38] Venegas, R.; Boutin, C.; Umnova, O. Acoustics of multiscale sorptive porous materials. *Phys Fluids* 2017; 29:082006.
- [39] Venegas, R.; Boutin, C. Acoustics of permeable heterogeneous materials with local non-equilibrium pressure states. *J Sound Vib* 2018; 418:221–239.
- [40] Venegas, R.; Boutin, C. Enhancing sound attenuation in permeable heterogeneous materials via diffusion processes. *Acta Acust United Ac* 2018; 104:623–635.
- [41] Gourdon, E.; Seppi, M. Extension of double porosity model to porous materials containing specific porous inclusions. *Acta Acust United Ac* 2010; 96:275–291.
- [42] Zieliński, T. G. Numerical investigation of active porous composites with enhanced acoustic absorption. *J Sound Vib* 2011; 330:5292–5308.
- [43] Lagarrigue, C.; Groby, J. P.; Tournat, V.; Dazel, O.; Umnova, O. Absorption of sound by porous layers with embedded periodic array of resonant inclusions. *J Acoust Soc Am* 2013; 134:4670–4680.
- [44] Groby, J. P.; Lagarrigue, C.; Brouard, B.; Dazel, O.; Tournat, V.; Nennig, B. Using simple shapes three-dimensional rigid inclusions to enhance porous layer absorption. *J Acoust Soc Am* 2014; 136:1139–1148.
- [45] Groby, J.-P.; Lagarrigue, C.; Brouard, B.; Dazel, O.; Tournat, V.; Nennig, B. Enhancing the absorption properties of acoustic porous plates by periodically embedding Helmholtz resonators. *J Acoust Soc Am* 2015; 137:273–280.
- [46] Chevillotte, F.; Jaouen, L.; Bécot, F.-X. On the modeling of visco-thermal dissipations in heterogeneous porous media. *J Acoust Soc Am* 2015; 138:3922–3929.
- [47] Le, A.; Gacoin, A.; Li, A.; Mai, T. H.; Wakil, N. E. Influence of various starch/hemp mixtures on mechanical and acoustical behavior of starch-hemp composite materials. *Compos B Eng* 2015; 75:201–211.
- [48] Pan, G.; Zhao, Y.; Xu, H.; Ma, B.; Yang, Y. Acoustical and mechanical properties of thermoplastic composites from discarded carpets. *Compos B Eng* 2016; 99:98–105.
- [49] Ligoda-Chmiel, J.; Sliwa, R. E.; Potoczek, M. Flammability and acoustic absorption of alumina foam/tri-functional epoxy resin composites manufactured by the infiltration process. *Compos B Eng* 2017; 112:196–202.
- [50] Tiuc, A. E.; Nemes, O.; Vermesan, H.; Toma, A. C. New sound absorbent composite materials based on sawdust and polyurethane foam. *Compos B Eng* 2019; 165:120–130.
- [51] Opiela, K. C.; Zieliński, T. G. Microstructural design, manufacturing and dual-scale modelling of an adaptable porous composite sound absorber. *Compos B Eng* 2020; 187:107833.
- [52] Cosse, R. L.; Araújo, F. H.; Pinto, F. A. N. C.; de Carvalho, L. H.; de Moraes, A. C. L.; Barbosa, R.; Alves, T. S. Effects of the type of processing on thermal, morphological and acoustic properties of syntactic foams. *Compos B Eng* 2019; 173:106933.
- [53] Oh, J.-H.; Kim, J.-S.; Nguyen, V. H.; Oh, I.-K. Auxetic graphene oxide-porous foam for acoustic wave and shock energy dissipation. *Compos B Eng* 2020; 186:107817.
- [54] Umnova, O.; Tsiklauri, D.; Venegas, R. Effect of boundary slip on the acoustical properties of microfibrous materials. *J Acoust Soc Am* 2009; 126:1850–1861.
- [55] Boutin, C.; Geindreau, C. Estimates and bounds of dynamic permeability of granular media. *J Acoust Soc Am* 2008; 124:3576–3593.
- [56] Boutin, C.; Geindreau, C. Periodic homogenization and consistent estimates of transport parameters through sphere and polyhedron packings in the whole porosity range. *Phys Rev E* 2010; 82:036313.
- [57] Nematı, N.; Lee, Y. E.; Lafarge, D.; Duclos, A.; Fang, N. X. Nonlocal dynamics of dissipative phononic fluids. *Phys Rev B* 2017; 95:224304.
- [58] Tournat, V.; Pagneux, V.; Lafarge, D.; Jaouen, L. Multiple scattering of acoustic waves and porous absorbing media. *Phys Rev E* 2004; 70:026609.
- [59] Bécot, F. X.; Jaouen, L. An alternative Biot's formulation for dissipative porous media with skeleton deformation. *J Acoust Soc Am* 2013; 134:4801–4807.
- [60] ISO 10534-2:2001, Acoustics—determination of Sound Absorption Coefficient and Impedance in Impedance Tubes—Part 2: Transfer-function Method, International Organization for Standardization, Geneva, Switzerland, 2001.